Interannual and seasonal variability of NO_x observed at the Mt. Cimone GAW/WMO global station (2165 m a.s.l., Italy)

P. Cristofanelli[1], I. Gutiérrez[2], J. A. Adame[3], P.Bonasoni[1], M. Busetto[1], F. Calzolari[1], D. Putero[1], F. Roccato[1].

[1] National Research Council of Italy, Institute of Atmospheric Science and Climate, Via Gobetti 101, 40129 Bologna, Italy

[2] Integrated Sciences Department, Research Centre of Natural Resources, Health and the Environment (RENSMA), University of Huelva, Huelva, Spain

[3] Atmospheric Sounding Station. El Arenosillo observatory. Atmospheric Research and Instrumentation Branch. National Institute for Aerospace Technology (INTA). Mazagón-Huelva. Spain.

Abstract

In this work, we present and analyze a dataset of near-surface NO and NO_2 observations carried out at the Mt. Cimone WMO/GAW global station (CMN, Italy, 2165 m a.s.l.) from 2015 to 2018. The purpose of this work is to provide a first characterization of NO and NO_2 variability over different time scales, as well as to obtain preliminary information about transport processes able to affect the observed variability. NO was characterized by a peak in February - March (mean value: 0.08 ppb), while in summer the typical levels were near or lower than the detection limit. NO_2 values maximized in winter (0.32 - 0.37 ppb) and minimized in summer (0.21 ppb in June). The evident NO and NO_2 diel cycles point towards a joint role of vertical transport of air masses from the regional planetary boundary layer (PBL) and photochemistry.

We combined nighttime observations (less affected by direct transport from the regional PBL) and 3D back-trajectories, calculated by the FLEXTRA model, to analyze how long-range atmospheric circulation could impact NO_2 observations. Even if some caveats should be considered when commenting results from back-trajectory analysis (i.e. NO_x removal by oxidation processes not represented, possible residual impact of regional PBL air masses, impact of adding/removing a single year from the analysis), some robust outcomes can be considered: the atmospheric transport from northern Africa and the Mediterranean basin was tagged to baseline NO_2 values, while the highest values were related to atmospheric circulation overpassing central/western Europe (spring) and North Italy (spring and summer). Less robust relationship were found between high NO_2 values and air masses passing over central/western Europe (winter) and eastern Europe (winter and summer). On the other side, mountain thermal wind regime represents an important process for the occurrence of high NO_2 events by transporting polluted air masses from the regional PBL to CMN.

Our analysis suggested that it is not possible to define a unique set of O_3/NO_x threshold values able to discriminate the photochemical ages of air masses as done in previous studies; these values must be tuned as a function of the season and, possibly, of the measurement site.

Finally, we segregated CMN observations as a function of conditions representative for the presence of free tropospheric- or PBL-affected air masses: higher NO_x were observed under conditions representative for the transport of air masses from the regional PBL; the differences between the two regimes are maximized in winter for NO and in summer-autumn for NO_2.

Keywords: Mediterranean basin, nitric oxide, nitrogen dioxide, photochemical ages, air pollution, back-trajectories, open fires, free troposphere, PBL.

1. Introduction

The availability of mature and quality assessed observations of atmospheric composition chemistry is a pillar for the monitoring and detection of regional and global changes as well as for the investigation of atmospheric processes. NO_x (i.e. the sum of nitric oxide NO and nitrogen dioxide NO_2) plays an important role in controlling the molar ratio of tropospheric ozone (O_3) and hydroxyl radical (OH). It is involved in chemical reaction cycles during daytime, as well as in the nighttime chemistry of the planetary boundary layer (PBL). Among its multiple roles in atmospheric chemistry, NO_x represents a precursor for secondary aerosol and affects the acidity of precipitation (Schultz et al., 2015 and references therein). Peroxyacetyl nitrate (PAN) is a "reservoir" species for NO_x that allow re-emission far from emission source regions (e.g. Fischer et al., 2014). Focusing on the anthropogenic sources, NO_x is generated from a wide variety of processes in the lower troposphere: high-temperature combustion of fossil fuels, as well as lower temperature combustion of biomass (e.g. wildfires, agricultural fires, domestic heating). As being co-emitted by CO_2 when fossil fuels are combusted at high temperatures, NO_2 is particularly suitable for disentangling the role of anthropogenic recent emissions in affecting CO_2 variability (see e.g. Reuter et al., 2019).

The Mediterranean basin is recognized as a globally sensitive region to air pollution and anthropogenic climate change (Giorgi and Lionello, 2008; Monks et al., 2009): thus, it is particularly relevant to gather information about NO_x in this region. Near-surface NO_x observations were previously discussed by Cristofanelli et al. (2017) for a network of three atmospheric observatories in southern Italy, while Adame et al. (2014) assessed the "weekend-weekday" effect for NO_x in southern Spain over 2003–2008. Cuevas et al. (2015) and Adame et al. (2019) investigated the long-term trend of NO_2 in the Iberian Peninsula. Recently, Adame et al. (2020) discussed long-term NO_2 trends at the El Arenosillo coastal station in southern Spain, reporting the possible impact of alterations in the weather patterns associated with a warmer climate to the observed NO_2. In general, long-term NO_2 satellite observations revealed strongly decreasing NO_2 trends over Europe (e.g. Castellanos and Boersma, 2012; Colette et al., 2016; Georgoulias et al. 2019), which are the results of complex contributions from environmental policy and socio-economic changes. Although not located in the Mediterranean basin, NO_x observations carried out at the WMO/GAW global stations Zugspitze (2670 m a.s.l., German Alps) and Jungfraujoch (3580 m a.s.l., Swiss Alps) can provide good hints for interpreting NO_x variability at high-mountain peaks. Gilge et al. (2010) evaluated 13 years of NO_2 measurements at Zugspitze and Jungfraujoch, reporting a decrease of NO_2 between 1995 and 2007; signals of anthropogenic NO_2 emissions were found in the NO_2 weekly cycle at the latter site. Except for summer, when NO_x are rapidly converted by photochemical cycle to higher oxidized species, Pandey Deolal et al. (2012) reported high interannual variability of mean NO_x values at Jungfraujoch due to the occurrence of short and episodic pollution events.

The main purpose of this work is to provide a first characterization of NO and NO_2 variability at the Mt. Cimone WMO/GAW global station (GAW ID: CMN), in northern Italy. As being located at high altitude

(2165 m a.s.l.) over the Po basin, CMN represents a perfect site to investigate the baseline conditions of NO_x over the Mediterranean basin, and to assess the possible impact of anthropogenic emissions following different atmospheric transport (from the local to the long-range scale).

2. Materials and methods

2.1 Site description and measurement system

Mt. Cimone (CMN, 44°12' N, 10°42' E, 2165 m a.s.l.), is the highest peak of the northern Italian Apennines and overlooks the Po basin (towards NW-SE) and northern Tuscany (towards S-NW). The Mediterranean Sea is about 50 km to the SW of the measurement site (Figure 1). The closest inhabited areas are small villages (1500 inhabitants) placed 15 km from and about 1100 m below the observatory, whereas major towns (~400000 inhabitants) are situated in the lowlands about 60 km away (Bologna, Firenze). Mt. Cimone is characterized by a 360° free horizon that allows the air masses to reach the measurement site without any topographic channeling. Within several kilometers from the site there are no crops, and human activity is very limited.

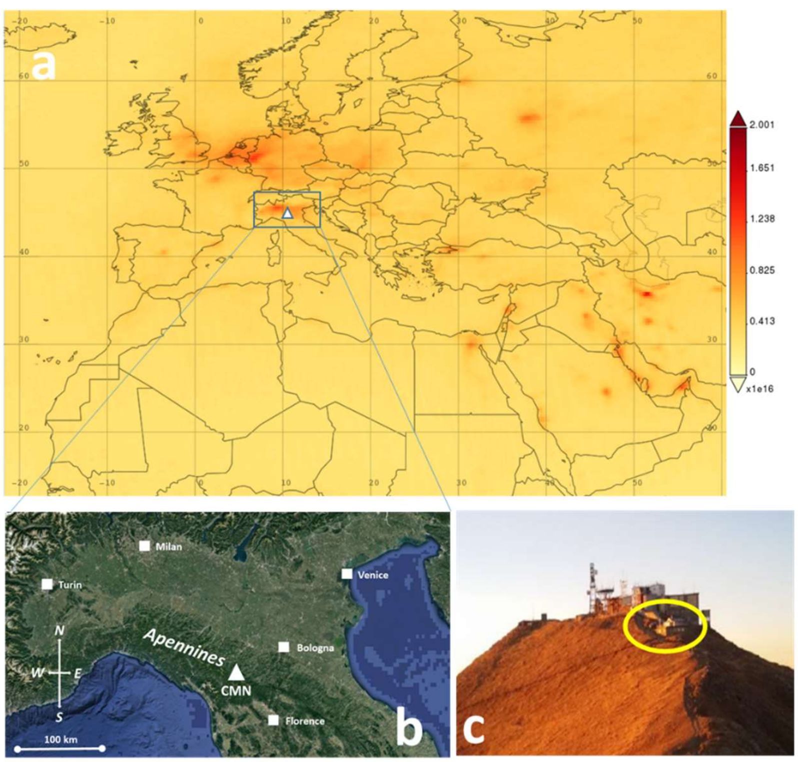

Figure 1. Time averaged map of NO_2 tropospheric column (total number of molecules) by TROPOMI (Tropospheric Monitoring Instrument) on-board of Sentinel-5 Precursor (S5P) satellite (Veefkind et al., 2012) for 2018 (a). The white triangle denotes the CMN location. A zoom to the northern Italy region is provided (b): the locations of the major urban areas (squares) are also reported. The summit of CMN with the "O. Vittori" observatory (circle) is also shown (c).

As reported by many previous investigations, the atmospheric observations carried out at CMN can be considered representative of the free tropospheric conditions of the Mediterranean basin / South Europe during the cold months (see e.g. Bonasoni et al., 2000), as well as during nighttime in the warm season. In particular, Henne et al. (2010) classified CMN as weakly influenced by surface fluxes from the European PBL. However, especially from April to September, the measurement site can be affected by "thermal" wind circulation and convective vertical transport of air masses. Indeed, during daytime, up-slope and valley winds together with diurnal growth of the PBL and related entrainment processes, can favor the vertical transport of polluted air to the measurement site (Cristofanelli et al., 2016; Cristofanelli et al., 2018), allowing air masses originated from northern Italy and affected by surface emissions to be caught at this measurement site. Conversely during nighttime, when the measurement site is usually well above the nocturnal boundary layer, CMN observations can be considered more representative of the background conditions or of aged emissions related both to long-range transport and to residual layers reminiscent of the daytime upward transport from the regional PBL. This makes the measurement site very suitable for investigating the baseline conditions of the Mediterranean troposphere, as well as the direct impact of surface emissions. To specifically provide evidence about the impact of air masses from the regional PBL to CMN, we analyzed the variability of water vapor and carbon monoxide (CO) at the measurement site. Specific humidity (SH) is a tracer widely used at mountain to diagnose the vertical transport of air masses from PBL to mountain sites (e.g. Cooper et al., 2020; McClure et al., 2016), while CO is one of the most used tracers for emissions related to the combustion of fossil fuel and biomass burning (e.g. Schultz et al., 2015). This analysis clearly shows that a systematic diurnal variability between nighttime and daytime during all the seasons for SH and CO exists, with maxima occurring around midday (Fig. 2). On the contrary, WS showed a typical reversed diurnal variation (i.e. lower values around midday). This pattern is similar to Mt. Bachelor (43.98°N 121.69°E, 2763 m a.s.l., Oregon, US; McClure et al., 2016), pointing out the daily modulation due to upslope (daytime) and downslope (nighttime) mountain winds. The different amplitudes of the SH and CO diurnal cycles among the seasons underpin the different efficiency of the thermal vertical transport processes in transporting polluted air masses from the regional PBL to CMN (maximized in summer and minimized in winter). As showed in previous works, the diurnal thermal transport of air masses from the regional PBL can significantly influence atmospheric composition at CMN (see Bonasoni et al., 2000; Cristofanelli et al., 2016; Cristofanelli et al., 2019). As concerning ozone (O_3), the average diurnal variation (mean daily maximum minus mean daily minimum) is minimized in winter and autumn (1 – 2 ppb) and increased in spring (3 ppb) and summer (6 ppb). The O_3 observations in afternoon-evening were higher with respect to the central part of the day due to the combination of vertical transport of air masses from the PBL and small (but not negligible) local photochemistry contribution.

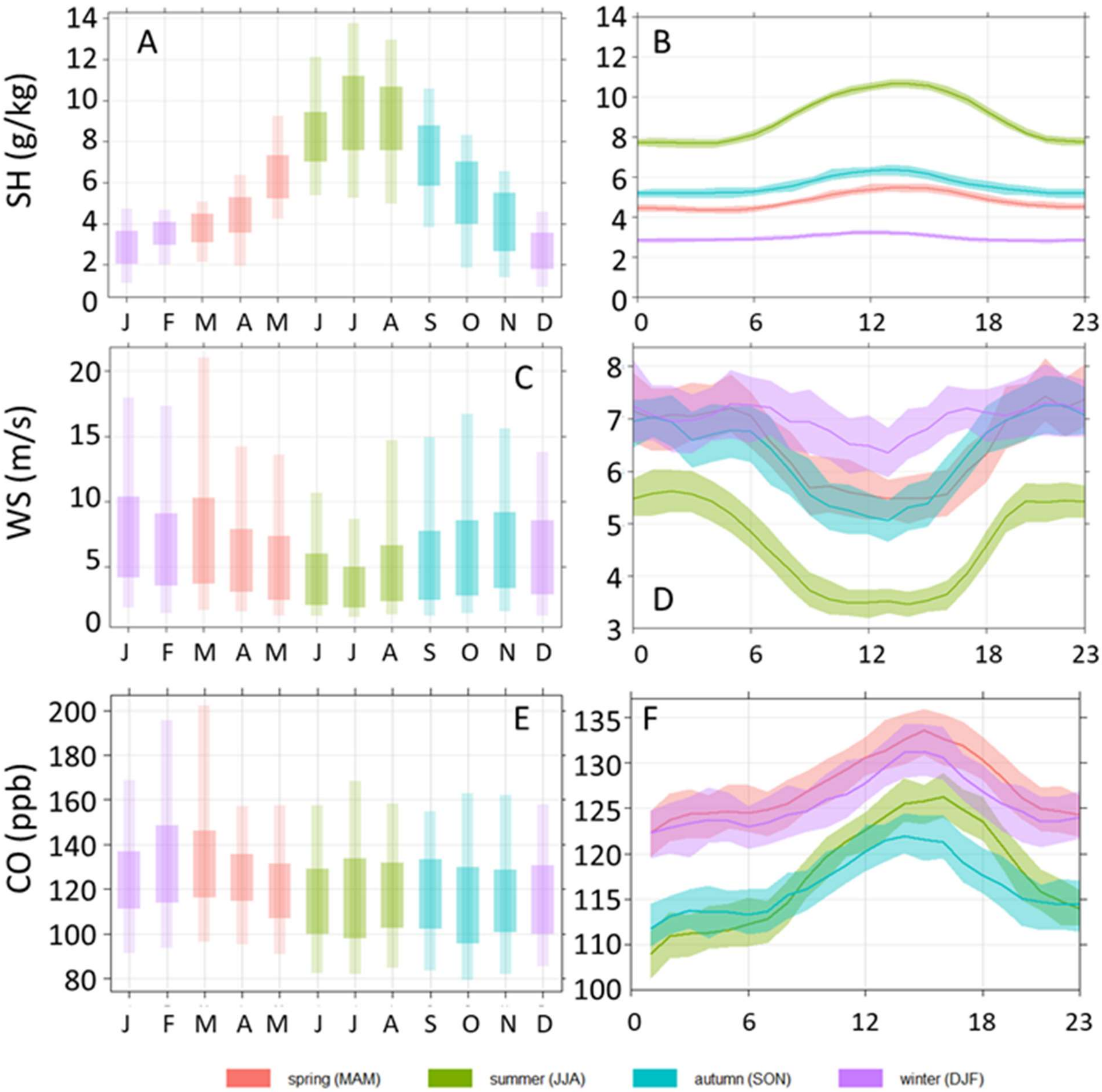

Figure 2. Yearly and diurnal variation of specific humidity (SH, plates A and B), wind speed (WS, plates C and D) and carbon monoxide (CO, plates E and F) at CMN (2015 – 2019). Plates A, C and E: bars and shaded areas represent 5th, 25th, 75th and 95th percentiles of hourly mean values. Plates B, D and F: lines and shaded areas report the mean values and the 95% confidence intervals, respectively. The color code indicates the different seasons.

During 2015–2018, NO and NO_2 observations were continuously carried out by using a chemiluminescence analyzer Tei42i-TL (Thermo Scientific) equipped with a photolytic converter (Blue Light Converter by Air Quality Design and Teledyne). During the investigated measurement period, two different converters were used. The first one (Photolytic NO_2 converter by Air Quality Design, Inc.) was characterized by an efficiency declining from 45% to 30% from January 2015 to September 2017 (please note that some short events of efficiency increase were observed). In November 2017, the converter was replaced by a new one (Blue Light Converter, Teledyne Technologies) with a higher conversion efficiency (about 95% at the beginning of the operations). During 2018 and 2019 the conversion efficiency experienced few abrupt events of decreases (probably related to the failure of led emitting diodes), leading to an efficiency of 75% at the end of 2019 (see Fig. SM1). Every 48 hours, zero and span checks are carried out for NO by using an external zero air source (Thermo Scientific dry air generator 1160 equipped with Purafill© and active charcoal scrubbers) and dilution of certified NO mixture in N_2 (5.0 ppm ± 2% by Messer Italia from January 2015, 4.8 ppm ± 2% by RISAM GAS from June 2016 and 5 ppm ± 3.5% by NPL from September 2017). It is not easy to determine the possible impact of the change of the reference standard to the analytical measurement uncertainty. Unfortunately, it was not possible to perform intercomparison exercises at the moment of the change of reference standards. However, all the reference standard producers provide uncertainty certification of the standard mixture that would assure consistency. To determine the efficiency of the NO_2 photolytic converter, gas phase titration (GPT) is used to titrate about 80% of the NO obtained by dilution. NO interferences caused by water vapor quenching and ozone interferences on NO and NO_2 have been corrected as recommended in Gilge et al. (2014). Along the years, the instrumental detection limit was assessed to range from 0.05 to 0.07 ppb for NO and to 0.08 to 0.10 ppb for NO_2. The total combined uncertainty for NO was calculated to be 4-5% by considering systematic contributions from NO standard uncertainty, random contributions from analyzer uncertainty (i.e. long-term and short-term repeatability), and random uncertainty of the dilution flow (i.e. standard deviation of dilution flow and standard deviation of calibration standard flow). By applying a simple uncertainty propagation to the determination of the NO_2 conversion efficiency from the total combined uncertainty of 5% for NO, a further 20% uncertainty should be considered for the NO_2 determination. As concerning the dilution system, both the dilution and calibration standard flows are checked once per year with external calibrated flowmeters. Moreover, the flowmeters in the dilution system were recalibrated every 2-3 years by a specialized private company. A general description of the data processing chain from the raw data to the submission to the ACTRIS-2 and WMO/GAW data repositories (http://ebas.nilu.no/) is provided by Naitza et al. (2020).

In the same period, carbon monoxide (CO) was measured by non-dispersive infrared (NDIR) absorption technique. The system was based on a Tei48C-TL analyzer (Thermo Environmental), which uses gas filter correlation technology for determining CO ambient molar ratio. With the aim of minimizing the possible influence of water vapor in the NDIR detection, the ambient air passed through a drying system (Nafion© dryer) and was then injected in the measurement cell. A span calibration was performed daily, while, every 6 months, a multipoint calibration was carried out by using a set of 6 NOAA standards. In this way, the measurements are referred to the WMO CO_X2014A calibration scale. The span value is 500 ppb and this concentration is obtained from the dilution of a 10 ppm CO standard cylinder (Producer: Messer Italia) with zero air produced by flowing ambient air through a carbonate cylinder filled with silica gel (to dry the ambient air) and a steel tube containing Sofnocat© 423. Tei48C-TL instrument is characterized by a strong drift of the zero value due to changes in ambient (room) temperature: to minimize the influence of temperature on the measurements, a specific software was designed and used to control the zero calibration, forcing the instrument to perform this calibration every 30 minute. A total uncertainty of 10% was assessed for these observations.

Near surface O_3 is measured by using an UV-absorption photometer Tei-49i (Thermo Scientific). Sampling flux control, as well as zero and span checks, were executed daily. The zero air was generated by using an activated charcoal cartridge, while an internal UV source was used to generate a span level of approximately 100 ppb. These checks were not used to calibrate the O_3 analyzer, but for performing regular functional tests and for identifying possible instrumental problems. The UV-analyser is regularly calibrated (roughly every 3 months) with a laboratory transfer standard (Tei 49i-PS, Thermo Scientific). On June 2018, the surface O_3 measurement system was audited by the GAW World Calibration Centre WCC-Empa. The bias with respect to the WCC travelling standard was lower than 1 ppb in the range 0-100 ppb, while the standard uncertainty of unbiased measurements was below 0.5 ppb (Zellweger et al., 2018).

At CMN, meteorological parameters were continuously observed by automatic integrated weather stations. During the investigation period, air-temperature, relative humidity and atmospheric pressure were recorded by a Rotronic MP101A-T4-W4W sensor (January 2015 - April 2016) and a Vaisala HMP-155 (May 2017 - December 2018). These data were used to calculate SH at the measurement site. Wind speed and direction were observed by a Vaisala WS-425 sonic anemometer along the whole investigation period. Solar radiation (wavelength: 350 – 1100 nm) observations are carried out by a commercial silicon cell pyranometer (Skye SKS110).

2.2 Air-mass trajectories and conditional probability calculations

The back-trajectories employed in this study were computed by the kinematic model FLEXTRA (Stohl et. al., 1995; Stohl and Seibert, 1998). For each day in the study period, four back-trajectories were calculated, using a runtime of seven days (168 hours), and starting at 00:00, 06:00, 12:00 and 18:00 UTC. Sub-grid scale processes, such as convection and turbulent diffusion, were not represented by the back-trajectory model. For these reasons, and to partially cope with such uncertainties, the back-trajectory endpoints at CMN were slightly shifted vertically. Thus, back-trajectories were calculated at three different altitudes (1700, 2200, 2500 m a.s.l.), with the CMN horizontal coordinates as starting point. The meteorological fields from the ECMWF (European Centre for Medium-Range Weather Forecasts) operational analysis were used as input. The spatial resolution is T106 (corresponding to a latitude/longitude resolution of 1.125° x 1.125°), while the temporal resolution is 6 hours. It should be clearly stated that, with such spatial resolution, it is not possible to obtain information about atmospheric transport processes occurring at the mesoscale, but we can obtain useful hints to depict the "synoptic" circulation and transport occurring at continental and hemispheric scales.

The conditional probability analysis aims to identify pollution sources by coupling back-trajectories with measurements information at the studied location (Ashbaugh et al, 1967). First, a selection of relevant events (i.e. observation periods) is made. Then, for every point i, j in a spatial grid, the conditional probability is defined as:

$$CP_{i,j} = m_{i,j}/n_{i,j}$$

where $m_{i,j}$ is the number of trajectories associated to the events and $n_{i,j}$ is the total number of trajectories crossing the point (i, j) during the whole investigation period. Hence, the higher the value of $CP_{i,j}$, the higher the probability that atmospheric transport passing over the grid point (i, j) systematically contributed to the events observed at the measurement location. In this work, the selection of events was firstly addressed by computing the daily mean molar ratio of NO_2 and selecting four percentile ranges: lower than 25th, 25th to 50th, 50th to 75th and higher than 75th. We only considered NO_2 observations in this analysis, because they can represent a good indicator of the emissions occurring at regional/continental scale (Gilge et al., 2010). In this way, we classified the atmospheric transport regimes that most likely contributed to each specific percentile range. This allowed to identify not only atmospheric transport associated to polluted air masses, but also those related to clean conditions. By this approach NO_2 is considered like a "passive" tracer that is far from the reality: NO_x can be removed by oxidation processes or re-emitted several days after emissions by reservoir species like PAN. Thus, the $CP_{i,j}$ analysis must be interpreted with great caution as a tool able to provide general indication about atmospheric circulation more or less favorable to the occurrence of high/low NO_2 values at CMN, without specific indications about the chemical source or removal processes occurring along the air mass transport. It should be argued that using 7-day long back-trajectories is a questionable choice when discussing variability of reactive species like NO_2 (having an average lifetime of a few hours in the PBL to a few days in the free troposphere). However, by this choice, we would consider also the possible contribution related to the long-range transport of reservoir species (like PAN) to the NO_2 variability observed at CMN. Also taking into account the results by Waked et al. (2018) about the impact of selecting different back-trajectory lengths to the $CP_{i,j}$ results, a further analysis was carried out by limiting the length of FLEXTRA back-trajectories to 3 days.

$CP_{i,j}$ maps were computed over a 1° x 1° latitude-longitude grid: only grid elements with at least 18 back-trajectories passing through were considered, to ensure the robustness of the conditional probability analysis (see Fig. SM2). Measurement data have been averaged over 3-hour time windows and centered at the time when the FLEXTRA back-trajectories were available, to allow the convolution with back-trajectories. To minimize the possibility that thermal wind circulation occurring during daytime could bias the $CP_{i,j}$ analysis based on the FLEXTRA back-trajectories (not able to resolve atmospheric transport occurring at mesoscale), only nighttime CMN observations (i.e. from 23:00 to 04:00 UTC+1) were considered.

2.3 Identification of free troposphere and PBL-influenced air masses

To select the observations periods representative of the free troposphere ("FT") or PBL-influenced air masses, we established a criterion based on the SH and WS data observed at CMN. Since free tropospheric air masses are expected to be characterized by a lower water vapor content and high wind speed (due to the downslope winds and synoptic-scale winds) with respect to PBL, we considered the measurement periods with SH lower than the monthly 25th percentile (calculated over the period 2015 – 2019) and WS higher than the 25th monthly percentile as representative of FT air masses. Conversely, to detect air masses more representative of the PBL, we selected the measurement period characterized by SH higher than the 75^{th} percentile and by WS lower than the 25^{th} percentile. This approach takes into account the seasonal variations of both SH and WS (Fig. 2) and, in spite of other approaches (e.g. Cooper et al., 2020; Bonasoni et al., 2000), does not impose a fix time windows (i.e. nightime vs daytime) for segregating data between "FT" and "PBL" regimes. It should be clearly stated that this approach is not aimed at characterizing which fraction of the time at CMN is influenced by "FT" or "PBL" air masses, but it is specifically devoted to detecting a subset of data representative of the two atmospheric regimes. As based on this analysis, the monthly averaged fraction of hourly observations representative for "PBL" air masses varied from 3% in February to 9% in July, while the selection of "FT" air masses showed a lower seasonal dependency with a monthly frequency ranging from 2.5% to 4.9% along the year (Fig, SM3). The majority (i.e. 47%) of "PBL"-representative data were collected from 10:00 to 15:00 UTC+1, while "FT"-representative data were mostly (i.e. 70%) collected at night (from 20:00 to 6:00 UTC+1).

3. Results and discussion

3.1 Overview and temporal evolutions for NO and NO_2

3.1.1 NO and NO_2 observations

First, a general characterization of NO and NO_2 over the study period was carried out. Figure 3 reports the statistical distribution of NO and NO_2 hourly mean values for the four years of investigation, while Figure 4 reports the time series of the monthly median and percentiles. For all years, NO showed a peak in the frequency around 0 ppb, clearly reflecting the detection limit of the experimental set-up, with a skewness towards higher values (not exceeding 0.20 ppb). The shape of the statistical distributions looks robust among the different years, with similar values for the 50^{th} (0.01 ppb) and 75^{th} percentiles (0.03 - 0.04 ppb). The interannual variability was more evident for the extremes (i.e. 95^{th} percentiles), which ranged from 0.12 ppb to 0.19 ppb. Only for 2017, we observed a flattening of the distribution peak around 0 ppb, which probably indicated a decline in the detection limit performance. Figure 3 reports the statistical distribution of NO and NO_2 for the different seasons. Overall, NO distribution is similar among the different seasons except for the 95^{th} percentile, which showed values 2-3 times higher in winter and spring (0.21-0.30 ppb) than in summer and autumn (0.06 - 0.11 ppb). NO_2 showed a skewed distribution centered around 0.10 ppb, but with an enhanced interannual variability with respect to NO (Fig. 3). Among the different years, the NO_2 mean average values ranged from 0.15 to 0.36 ppb, while 25^{th} and 50^{th} percentiles ranged from 0.05 to 0.19 ppb, and from 0.16 to 0.40 ppb, respectively. A rather different shape of the data distribution was evident for 2016 (see also Fig. 4), with a less evident distribution peak and an overall shift of data population towards higher values (Fig. 3). This is reflected in the interannual variability of the statistical parameters: 2016 showed the highest values for every NO_2 percentile (Table SM1), thus implying an overall shift of the population distribution by ~ 0.1 ppb.

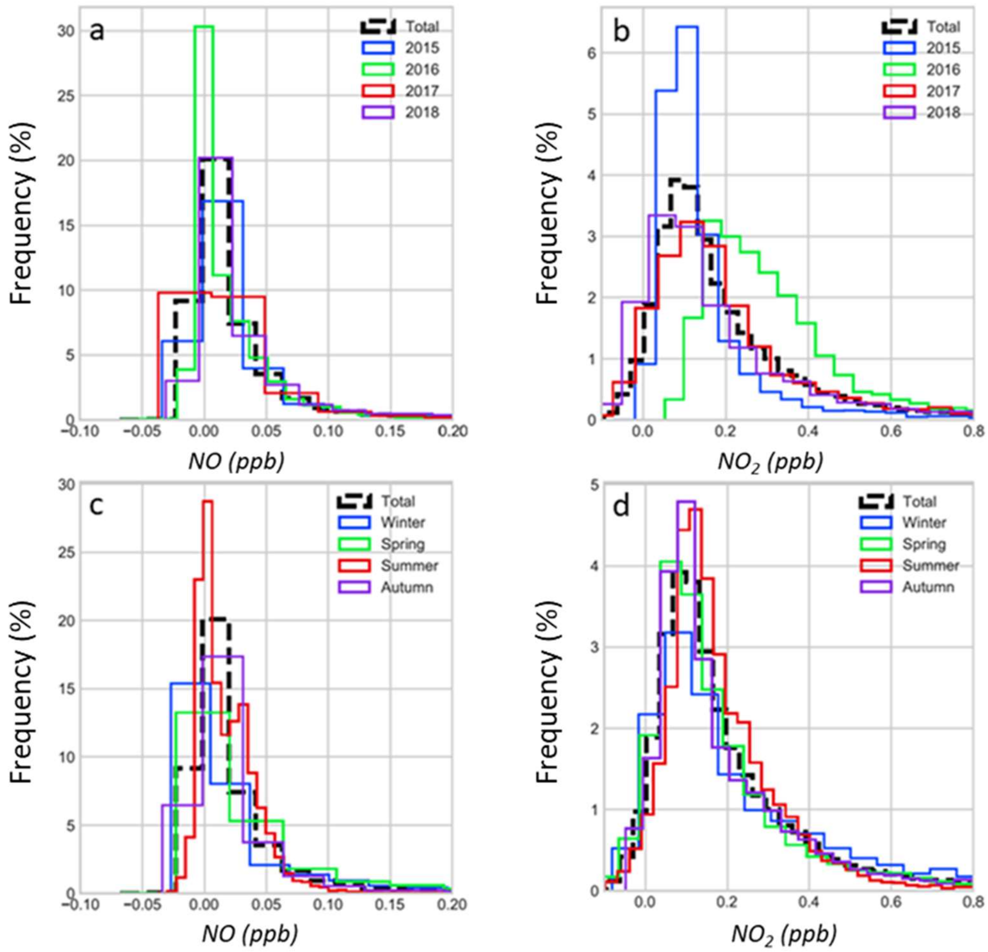

Figure 3. Normalized annual (a-b) and seasonal (c-d) distributions for NO (a - c) and NO_2 (b – d) hourly mean values.

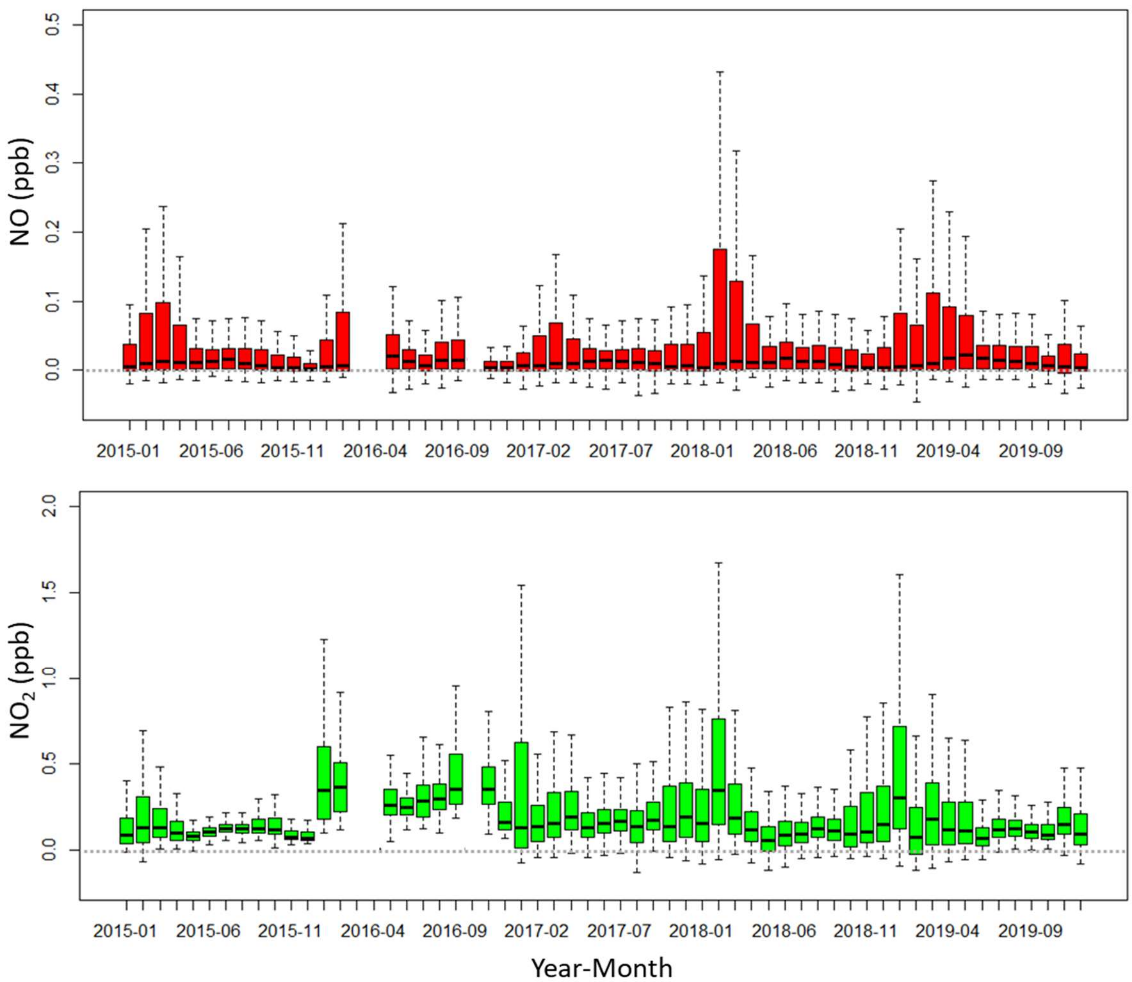

Figure 4. Time series of monthly median (thick lines) and percentiles (5th, 25th, 75th and 95th) for NO and NO_2 at CMN.

With the purpose of better characterizing the measurement site, as well as the NO_x dataset, Figure 5 reports wind direction distribution of NO and NO_2 observations belonging to the specific percentile ranges. In agreement with CMN climatology (Cristofanelli et al., 2018), over 2015–2018 two main wind sectors are evident: NE (N - NE and NE) and SW (S - SW, SW, W - SW). Regarding wind speed, the NE sector is associated with average values of 8 - 10 m s^{-1}, while SW sector presents higher values (14 - 18 m s^{-1}). In general, for both trace gases, the NE sector is characterized by most measurements lying between the 50th and the 100th percentiles. In particular, the N - NE sector is characterized by a large fraction of observations within 75th - 100th percentiles (especially for NO_2). In contrast, SW and SSW sectors show a stronger occurrence of observations in the lower half of percentiles (0th - 50th). This behavior is similar for all seasons (see Fig. SM4), but for N - NE sectors the occurrence of data belonging to the higher ranges (90th - 100th percentiles) is maximized in winter and summer.

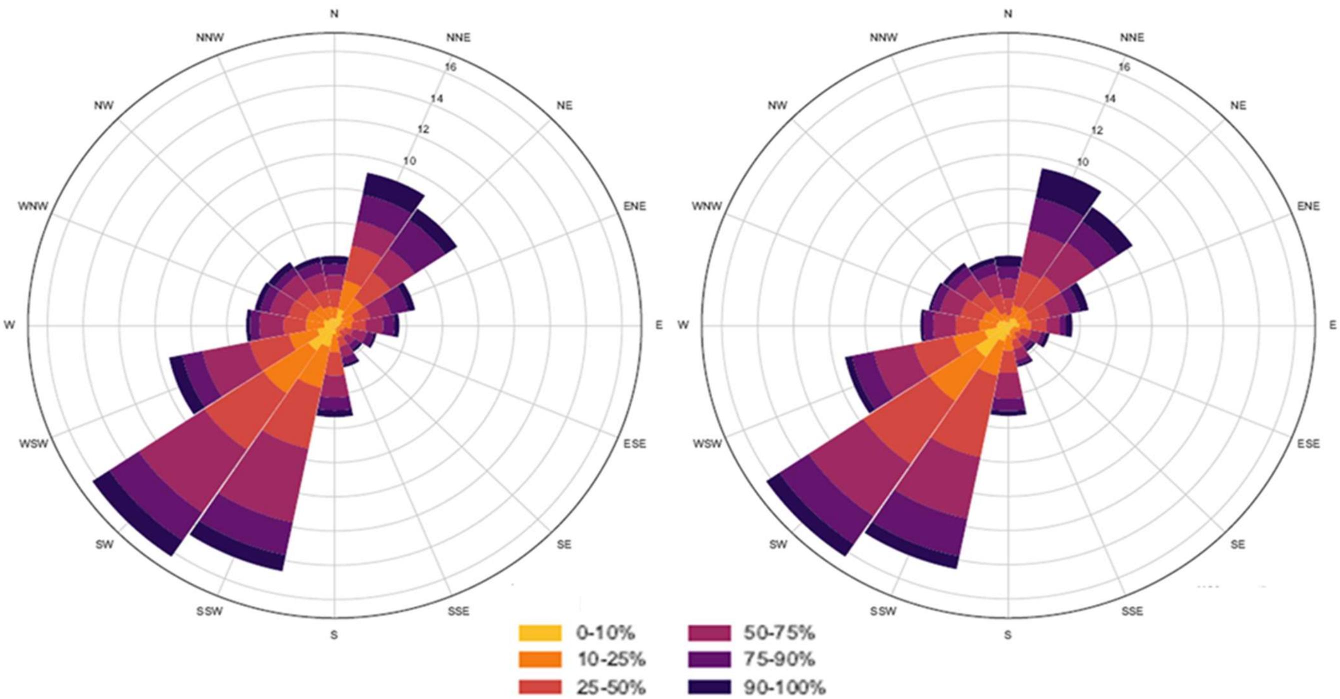

Figure 5. Wind distribution for NO (left) and NO_2 (right) divided in 16 wind sectors. The radius denotes the average wind speed (in m s^{-1}) associated to each wind direction. The colored areas represent the fraction of the data belonging to specific NO and NO_2 percentile range (calculated over the whole measurement period) for each wind sector.

3.1.2 Typical temporal variability of NO and NO_2

Figure 6 shows the annual variation of monthly mean values for NO and NO_2 for each year from 2015 to 2019, while Figure SM5 in the supplementary material provides overall median and main percentile values over the full period 2015 - 2019. Depending on the single year, NO was characterized by a peak in February - March (average values: 0.08 ppb) and a minimum (lower than 0.02 ppb) in July. As deduced by the monthly 95% confidence levels, also the range of variability increases in autumn-winter and decreases in spring-summer. This is also testified by the large differences between median (Fig. SM5) and mean (Fig. 6) values, indicating that the occurrence of high NO episodes affected the mean average values. The same features can be observed for NO_2, which maximized in winter (January – February: 0.32 - 0.37 ppb) and minimized in June (0.21 ppb). This is expectable due to a major accumulation in the lower atmospheric layers associated to the stable boundary layer, and less destruction by photochemical processes with respect to summer. Even if they are covering different years, the NO_2 seasonal variation at CMN is comparable, in both amplitude and absolute values, with that observed at the high Alpine station of Jungfraujoch in 1997 - 2008 (Gilge et al., 2010) and 1998 - 2009 (Pandey Deolal et al., 2012). CMN observations seem to be in good agreement with Okamoto and Tanimoto (2016) who reported annual NO_x cycles varying from 0.7 ppb in autumn-winter to 0.3 ppb in summer at the Zugspitze (Germany) alpine station. The annual cycle of NO is much more pronounced than for NO_2 and can be explained by the higher reactivity of NO with respect to NO_2. As deduced by the analysis of NO and NO_2 statistical distributions (Sect. 3.1.1), the increase in the average values observed during winter-spring was affected by the occurrence of "extreme" events (i.e. values higher than the 95th percentile).

The analysis of NO_2 as a function of the single months (Fig. 6) showed constantly higher values in May – September 2016 with respect to the other years. However, the inspection of the NO_2 zero readings and of the converter efficiency values (which decreased from above 45% to 40% along the year, see Figure SM1) did not point out any obvious analytical problem. Moreover, it should be noted that the deviation of NO_2 values during May – September 2016, with respect to the remaining period, is comparable with the NO_x variability observed for specific seasons/years also at other measurement sites (see e.g. Pandey Deolal et al., 2012).

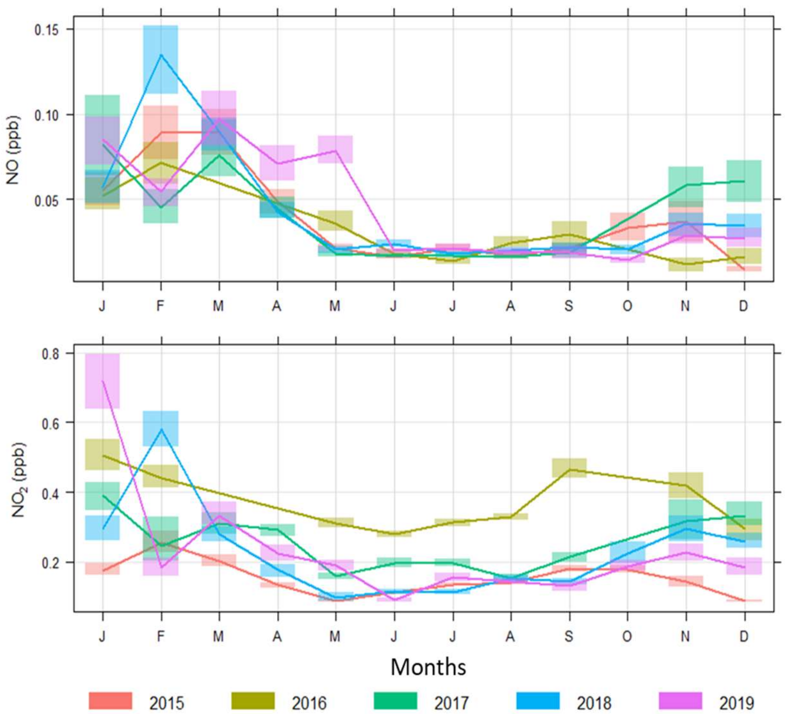

Figure 6. Monthly NO and NO_2 during years 2015 - 2018. The vertical bands represent the 95% confidence level of the mean average values.

A possible (not definitive) explanation for the high NO_2 values observed in 2016 can be related to enhanced transport from the PBL (July and August 2016 showed among the highest fraction of PBL-segregated air masses with respect to years 2015 – 2019), nevertheless this possible enhanced transport from PBL is not reflected by the CO variability. A further possibility can be related to the impact of regional and long-range atmospheric circulation: a preliminary inspection of the available outputs by the Lagrangian particle dispersion model FLEXPART (Stohl et al., 1998, 2005), driven by operational three-hourly meteorological data at 1°x 1° resolution from the European Centre for Medium-Range Weather Forecasts (ECMWF), revealed for summer 2016 a relatively larger contribution of air masses originated over East Europe and North Italy as well as a decreased contribution of long-range transport from the northern hemisphere with respect to year 2015 (here not shown).

For the different seasons, the NO_2 frequency distributions (Fig. 3 and 6) showed a higher occurrence of high values during winter, indicating an enhanced occurrence of transport of air masses rich in NO_2. With the aim of better discussing the interannual variability of NO_2 at CMN, Figure SM6 reports the seasonal average values together with median and percentiles (25th and 75th) for years 2015 – 2019. Excluding 2016, the variability of the NO_2 median values and 25th percentiles appear to be comparable among the different years. On the other side, in winter and spring, the NO_2 mean values and the 75th percentiles showed a larger variability, probably suggesting the occurrence of pollution episodes at CMN. The relatively low mean values and 75th percentile suggested a limited occurrence of pollution events in 2015 compared to the other years.

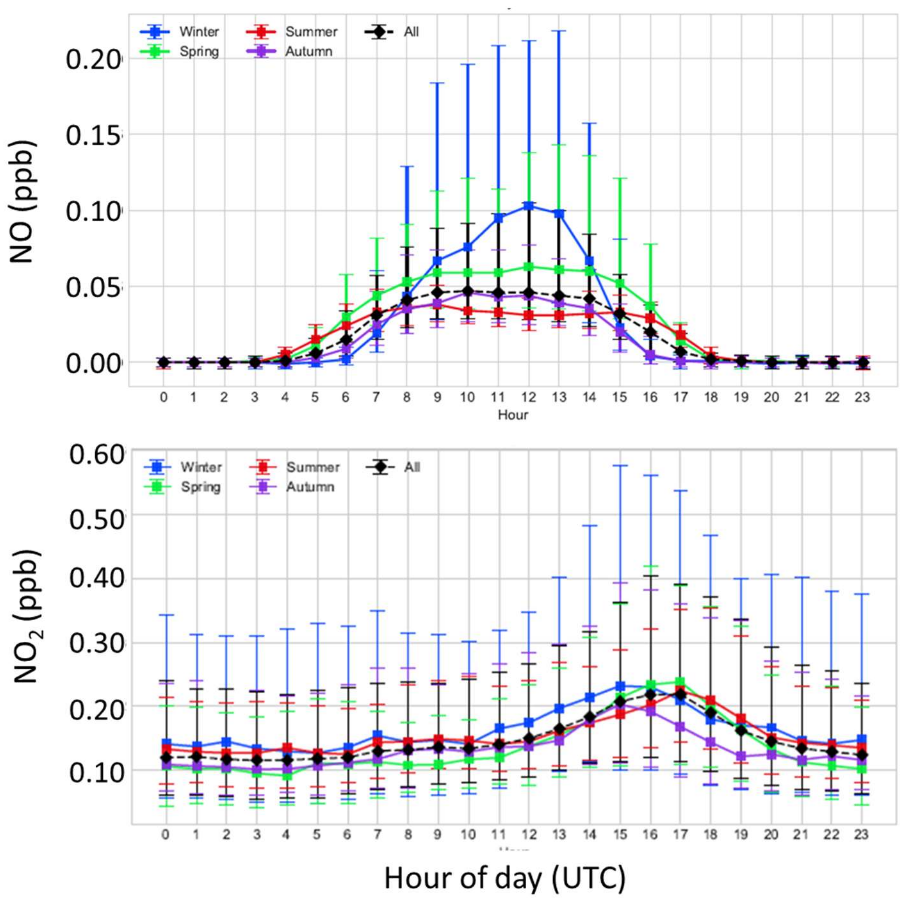

Figure 7. Averaged (2015 - 2018) diurnal cycles for NO (upper plate) and NO_2 (bottom plate) as a function of the four seasons: winter (DJF), spring (MAM), summer (JJA) and autumn (SON). For each hour, the mean mixing ratios are reported together with the standard deviation (vertical bar).

The investigation of diel variabilities can provide hints for interpreting the role of thermal wind circulation, PBL dynamic and photochemistry in the variability of NO and NO_2 (Fig. 7). In agreement with other mountain sites (see Reidmiller et al., 2010), NO shows a peak during mid-day due to the photolysis of NO_2 to NO. A strong dependence as a function of the seasons is evident for the averaged NO diel cycle: the shape of the cycle flattens and broadens moving from winter (highest NO diurnal values) to summer (lowest NO diurnal values). In particular, the diel variability during spring was in a relatively good agreement with that reported for Jungfraujoch by Zanis et al. (2000). The flattening of the NO diel shape in spring-autumn can be related to an increased impact of OH radical, which promotes a more efficient removal of NO (by HO_2, RO_2, O_3) with respect to the winter months. Also, the variability of hourly values strongly decreased from winter to summer, as deduced by the hourly standard deviation values. The averaged diel cycles for NO_2 showed less variability depending on the seasons, even if some specificities can be observed. For all seasons, an increase was observed from the late morning to the evening, with maximum values from 15:00 to 17:00 UTC+1. This behavior can be related both to photochemistry and to PBL dynamics, which favor the advection of more polluted air masses from the PBL during this time window at CMN, especially during the warm months (see Cristofanelli et al., 2016). The NO/NO_2 ratio shows a seasonal variability with high values in winter-spring and low values in summer-autumn (Fig. SM7). The values in spring, higher compared to autumn, are in agreement with the results from Mt. Bachelor (Reidmiller et al., 2010). Reidmiller et al. (2010) suggested that nitrogen-containing species adsorbed and dissolved in the mountain snowpack can be photolyzed to release NO_x (e.g. Honrath et al., 2000; Pandey Deolal et al., 2012) potentially contributing to NO_x emission and explaining the high NO/NO_2 ratios observed at Mt. Bachelor in spring. To investigate the possibility that snowpack denitrification processes can affect CMN observations in spring and winter, we analyzed the diurnal NO and NO_2 maximum as a function of the occurrence of snow precipitation and snow depth observed on a daily basis at Pian Cavallaro (located at 1850 m a.s.l., just below CMN) by "Carabinieri Forestali – Servizio Meteomont" (http://www.meteomont.gov.it/infoMeteo/). As an example, during year 2015 some of the highest NO events (22^{nd} – 26^{th} January, 6^{th} and 24^{th} February, 3^{rd} March, 8^{th} April) were observed during or just after snow precipitation events (Fig. SM8). In concomitance with the snow events also NO_2 increases were observed, but with lower amplitude than NO. It should be noted that several other NO peaks appeared not related with snow events, and no clear relationship is evident between the NO peaks and the daily solar radiation maximum observed at CMN. Moreover, the analysis of NO (and NO_2) daily peak as a function of wind speed did not reveal any evident anti-correlation with the observed NO values, as expected in the case of NO_x emission from the local snowpack (e.g. Pandey Deolal et al., 2012). By removing the days affected by fresh snow precipitation from the dataset, no evident deviations with respect to the results provided by Figure SM7 are obtained, thus suggesting that (if occurring) local snowpack denitrification plays a limited role in determining NO_x variability at CMN. Further specific efforts are needed to better assess the possibility that snow pack denitrification processes can affect the occurrence of high NO/NO_2 at CMN during winter.

Gilge et al (2010) pointed out the existence of weekly cycles in NO_2 at the Jungfraujoch station during all seasons, with maxima during the working days and minima on Sundays, thus tracing a direct impact of anthropogenic emissions from the regional PBL. A similar NO_2 weekly cycle affected CMN observations in spring, summer, and autumn (not shown). The amplitude of this weekly cycle minimized in summer (less than 0.05 ppb) and maximized in autumn (0.10 ppb).

3.2 NO_2 large-scale transport at CMN

The existence of a multi-year dataset at CMN allows to perform systematic studies to investigate the possible impact of large-scale transport regimes in affecting NO_2 observations. For each season, we calculated the $CP_{i,j}$ fields (see Sect. 2.2) for the four different NO_2 and CO quantiles observed at CMN (Fig. 8 and Fig. 9, respectively). This allowed to gain an overview about the role played by different air-mass transport regimes in NO_2 variability. The comparison with CO results can provide hints to support the role of combustion as source of NO_2 variability observed at CMN. Due to the strong seasonality of NO_2 and CO, the percentile ranges of each season were applied independently: this allowed to better identify clean and polluted sources. To minimize the interference by daytime upward air-mass transport from the PBL, only nighttime values were considered. This analysis was carried out (i) by considering the total length of available back-trajectories (i.e. 7 days, Fig. 8A and 9A) and (ii) by considering a limited length of 3 days for the back-trajectories (Fig. 8B and 9B).

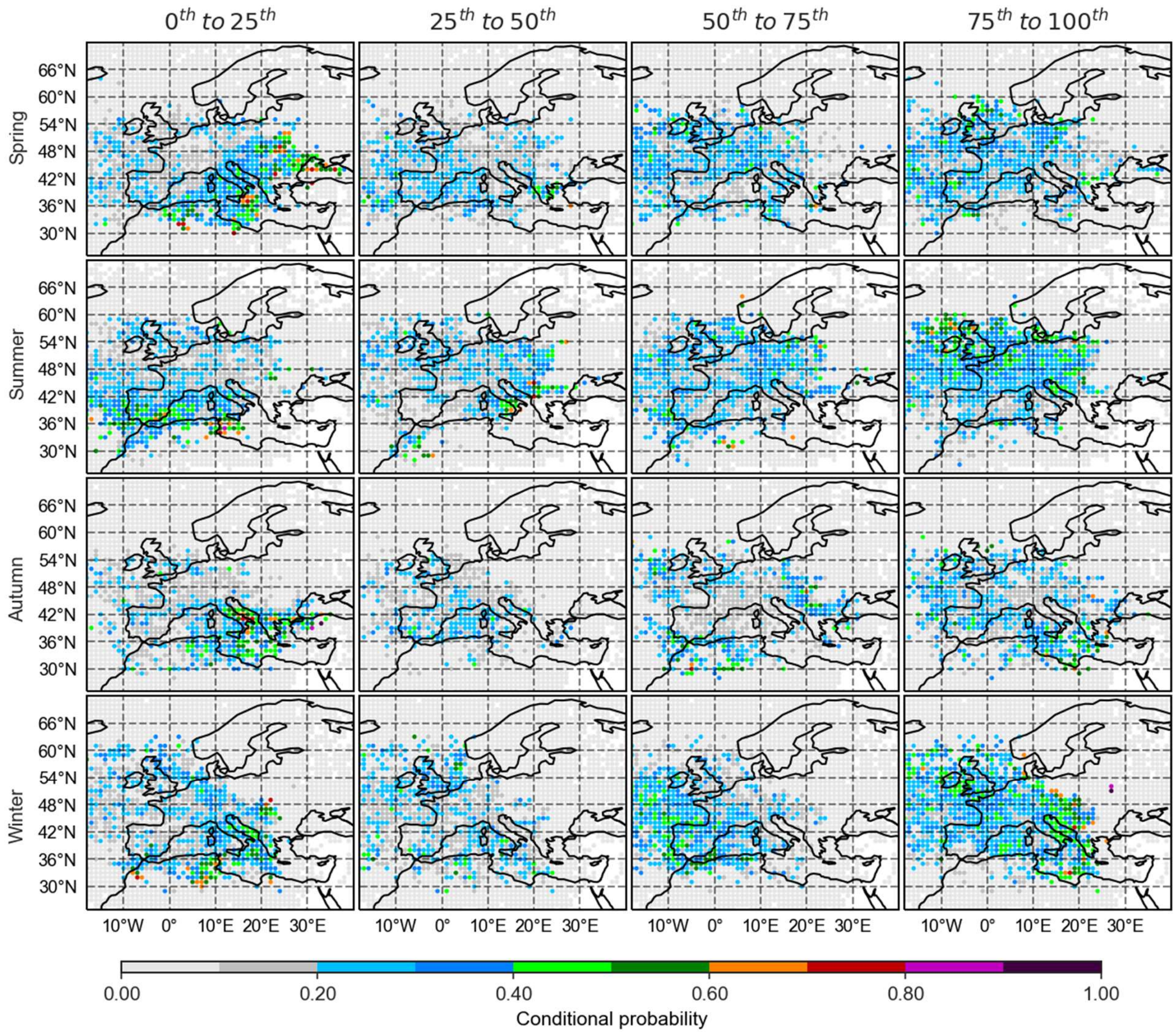

Figure 8A. For each quantile of NO_2 at CMN (columns), the spatial distribution of conditional probability $CP_{i,j}$ reconstructed using FLEXTRA back-trajectories is reported for each season (rows).

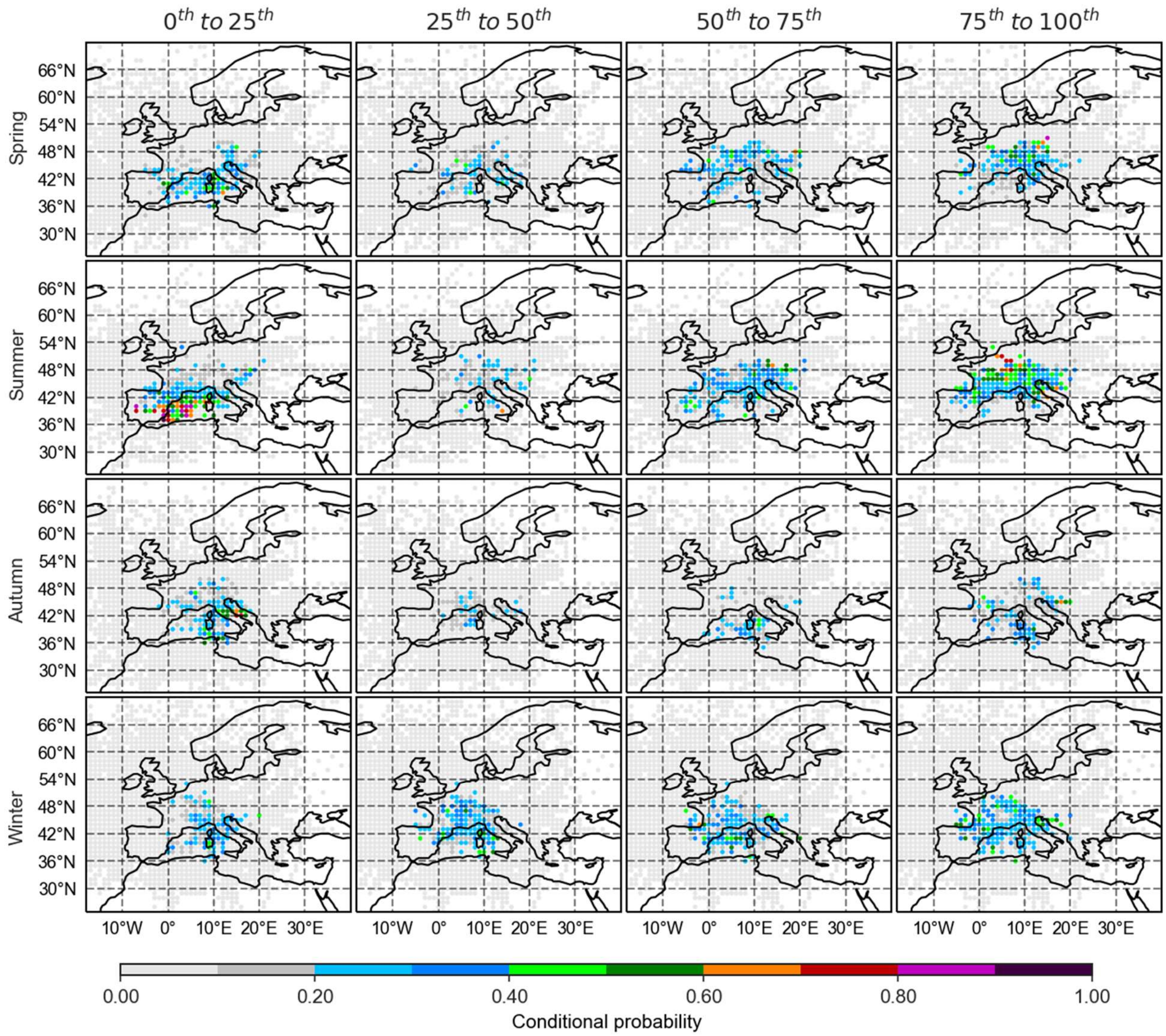

Figure 8B. For each quantile of NO_2 at CMN (columns), the spatial distribution of conditional probability $CP_{i,j}$ reconstructed using FLEXTRA back-trajectories of 3-day length is reported for each season (rows).

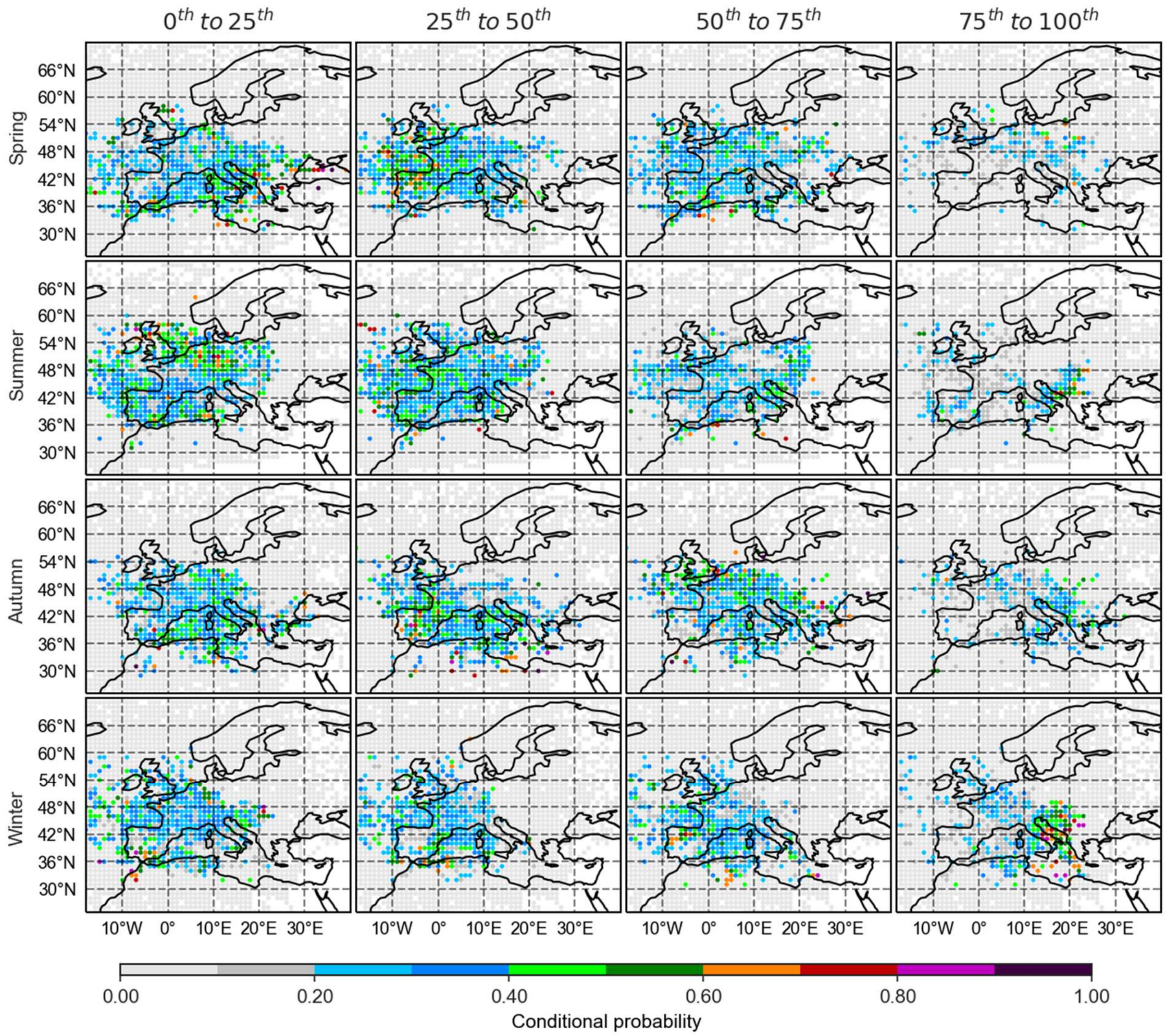

Figure 9A. For each quantile of CO at CMN (columns), the spatial distribution of conditional probability $CP_{i,j}$ reconstructed using FLEXTRA back-trajectories is reported for each season (rows).

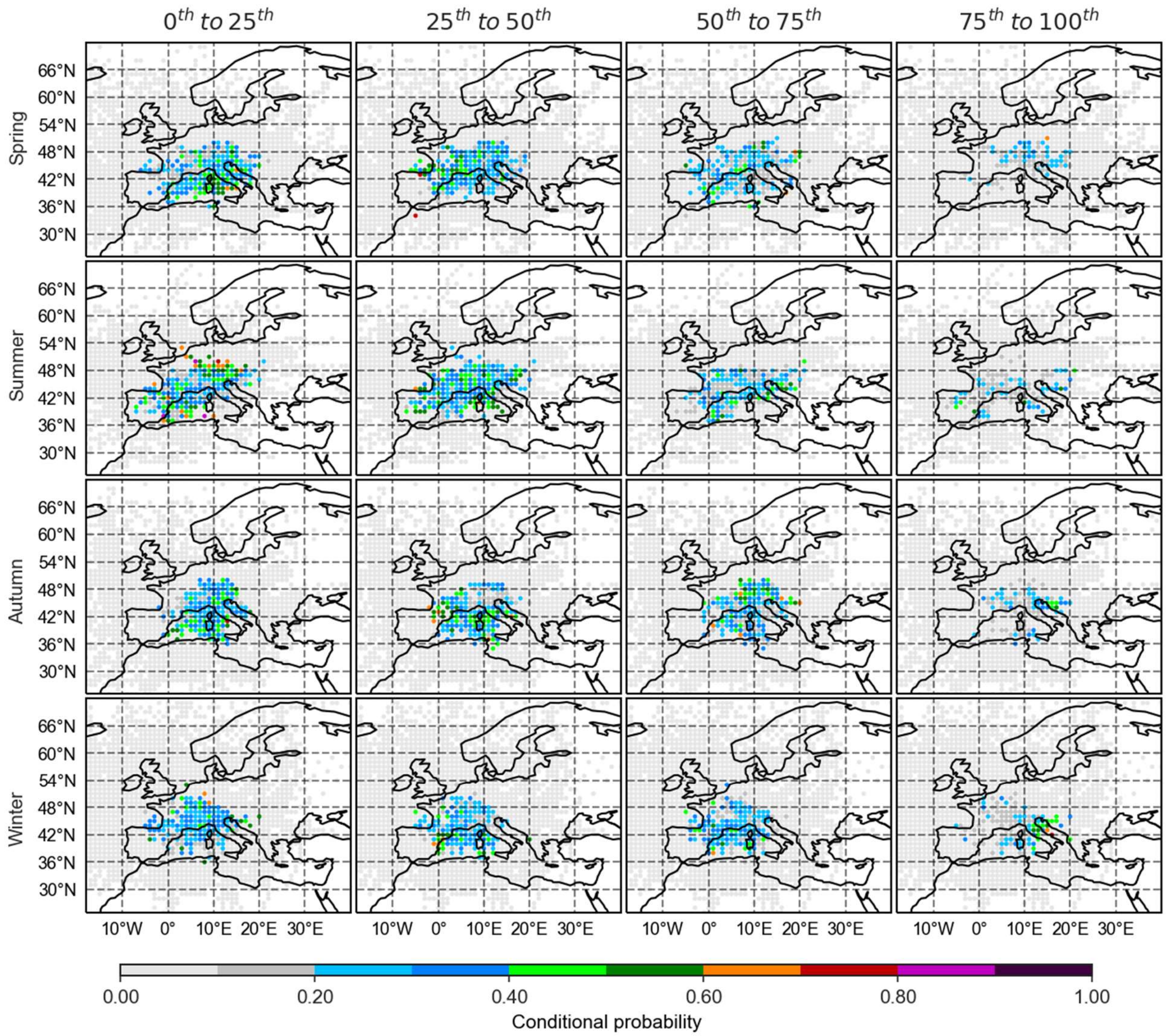

Figure 9B. For each quantile of CO at CMN (columns), the spatial distribution of conditional probability $CP_{i,j}$ reconstructed using FLEXTRA back-trajectories of 3-day length is reported for each season (rows).

In spring, high $CP_{i,j}$ values were tagged to regions in northern Africa, Mediterranean basin (mainly in Southern Italy) and eastern Europe, for air masses characterized by low NO_2 content at CMN (0^{th} to 25^{th} percentile). This feature is somewhat reproduced also for CO with $CP_{i,j}$ values higher than 0.4 over the same regions. Not clear signals can be obtained for the higher NO_2 and CO quantiles: a large portion of the geographical domain is characterized by $CP_{i,j}$ values higher than 0.3 - 0.4.

In summer, for the NO_2 observations falling in the lowest quantile, the highest $CP_{i,j}$ values were detected over the southern Iberian Peninsula and the Mediterranean basin. This is true also for CO, but with high $CP_{i,j}$ values observed for air masses travelling over continental Europe (probably tracing long-range transport from northern latitudes). For the highest NO_2 quantile (75^{th} to 100^{th}), the highest $CP_{i,j}$ values (i.e. > 0.4) were obtained over Benelux, eastern Europe (Poland, Ukraine, Belarus) and UK. For the CO highest quantile, high $CP_{i,j}$ values were detected only over eastern Europe.

During Autumn, high $CP_{i,j}$ characterized the central Mediterranean basin for the lowest NO_2 quantiles (the same is observed for CO), while univocal features were not obtained for the highest quantiles: for the NO_2

observations falling within the third quantile, two broad areas (i.e. eastern Europe and northern western Africa) showed values up to 0.4, while for the upper quantile similar high $CP_{i,j}$ values characterized the Iberian peninsula and the central Mediterranean basin. $CP_{i,j}$ values higher than 0.4 were observed for CO over eastern Europe for the third quantile (but not over Africa) as well as over central continental Europe. As concerning winter, for the lowest NO_2 quantile, high $CP_{i,j}$ values characterized northern Africa, eastern Europe and the central Mediterranean basin. The same is observed for CO (except than for the Mediterranean basin). The highest $CP_{i,j}$ values (higher than 0.4) were generally identified over the eastern domain (i.e. for longitudes > 10°E) for the highest CO and NO_2 percentiles (75^{th} – 100^{th}).

As reported in Section 3.1.2, when compared with the other years, 2016 was characterized by higher NO_2 values at CMN from May to September. To assess how this would influence the $CP_{i,j}$ analysis, we made a sensitivity study by calculating spring – autumn $CP_{i,j}$ only using 2015, 2017 and 2018 data (Fig. SM9). The results appeared robust between the two calculations, except for the following points:

- for spring, the sensitivity calculation did not show high $CP_{i,j}$ over the Atlantic for the highest NO_2 percentiles;
- for summer, the sensitivity calculation did not show high $CP_{i,j}$ over the UK and Ireland for the highest NO_2 percentiles, while the signal over Eastern Europe and (especially) Benelux was still visible;
- for autumn, the sensitivity calculation did not show high $CP_{i,j}$ over the central Mediterranean basin (a $CP_{i,j}$ up to 0.4 was only visible over Benelux and the Balkan Peninsula for the highest NO_2 percentiles)

A further sensitivity study was carried out to evaluate the impact of using short back-trajectories (3-day long) to the $CP_{i,j}$ results (Fig. 8B). This would help in characterizing more clearly the impact of regional sources and their geographical origins to the NO_2 variability as well as in evaluating the robustness of the results achieved by the analysis of 7-day long back-trajectories. During spring and summer the lowest NO_2 percentiles (0^{th} to 25^{th}) were tagged to air masses from the western Mediterranean basin, while the highest NO_2 percentiles (75^{th} to 100^{th}) were related to high $CP_{i,j}$ values over North Italy and central/western Europe (spring and summer). During autumn a cluster of high $CP_{i,j}$ values characterized Italy and the western Mediterranean basin for the lowest NO_2 percentiles (0^{th} – 25^{th}), while univocal results were not achieved in winter. These results were confirmed by the CO analysis for the lowest percentiles but only partially for the highest ones: for the highest CO quantiles, high and coherent $CP_{i,j}$ values were only observed over central/western Europe in spring.

3.3 Identification and analysis of events with high NO_2

To further investigate the behavior of NO_2 pollution events, a selection of days with high NO_2 measurements was performed. With the purpose to remove the effect of the seasonality on the detection of high NO_2 events, we subset the dataset as a function of the seasons. The NO_2 anomalous episodes were defined as those days in which the daily average exceeded the seasonal average by 2 σ. This is equivalent to select the days with daily NO_2 average exceeding the 96th quantile. 56 days were identified as "anomalous" during 2015–2018: from 12 (autumn) to 16 (winter), on a seasonal basis (see Table 1). Single-day events represented from 28% (in winter) to 50% (in autumn and spring) of the anomalous NO_2 events, while spring and winter were the only seasons reporting anomalous NO_2 events lasting more than 2 days (36% and 62%, respectively). An evident interannual variability affected the occurrence of high NO_2 events: 1 day was detected as "anomalous" in 2015, 21 days in 2016, 15 in 2017, and 14 in 2018. This variability is particularly evident for summer and spring, which reported a prevalence of events in 2016 and 2017, respectively.

Year	*Summer*	*Autumn*	*Winter*	*Spring*	*Whole year*
2015	0	0	0	1	1
2016	13	2	5	1	21
2017	1	3	6	10	20
2018	0	7	5	2	14
Whole period	14	12	16	14	56

Table 1. Temporal distribution of the number of "anomalous" NO_2 days for each season and year.

In general, the anomalous NO_2 events were characterized by lower air-temperature, lower atmospheric pressure, and higher wind speed with respect to the "not anomalous" days (Fig. SM10). This would suggest that the role of "stagnant" atmospheric conditions in favoring the occurrence of these high NO_2 events is unlikely. Further hints for the attribution of the anomalous NO_2 events can derive from the analysis of the NO and NO_2 daily cycles in the different seasons (Fig. 10). In winter, spring and autumn, the daytime (i.e. 10:00 - 17:00 UTC+1) NO values increased by about one order of magnitude with respect to the not anomalous conditions (see Fig. 7), while a 2-fold increase was observed in summer. On average, clear diel cycles were evident for both trace gases during the high NO_2 events. In summer and spring, the observed daily variability mimics the one observed for the not anomalous days. The high NO values, and the presence of a strong diel cycle for NO_2, would suggest the impact of "fresh" emissions occurring over northern Italy, possibly related with the thermal transport from the regional PBL. Weather conditions suitable for this transport occur mainly in summer, causing a high number of anomalous events in this season. A similar variability is also observed in autumn (i.e. higher NO_2 values during afternoon-evening), possibly suggesting a role of air mass transport from the regional PBL also in this season. The presence of a robust diel cycle (i.e. daytime vs nighttime differences exceeding the 95% confidence level) was found for CO during summer and autumn (Fig. 10), further supporting the role of diurnal transport of polluted air masses from the PBL. For winter and spring, not clear averaged diel CO cycles were evident for the anomalous NO_2 events at CMN (Fig. 10). Even if the role of air mass transport from the regional PBL cannot be excluded, this would suggest that the observed NO_2 variability can also be related to photochemistry or transport events occurring on longer time scales.

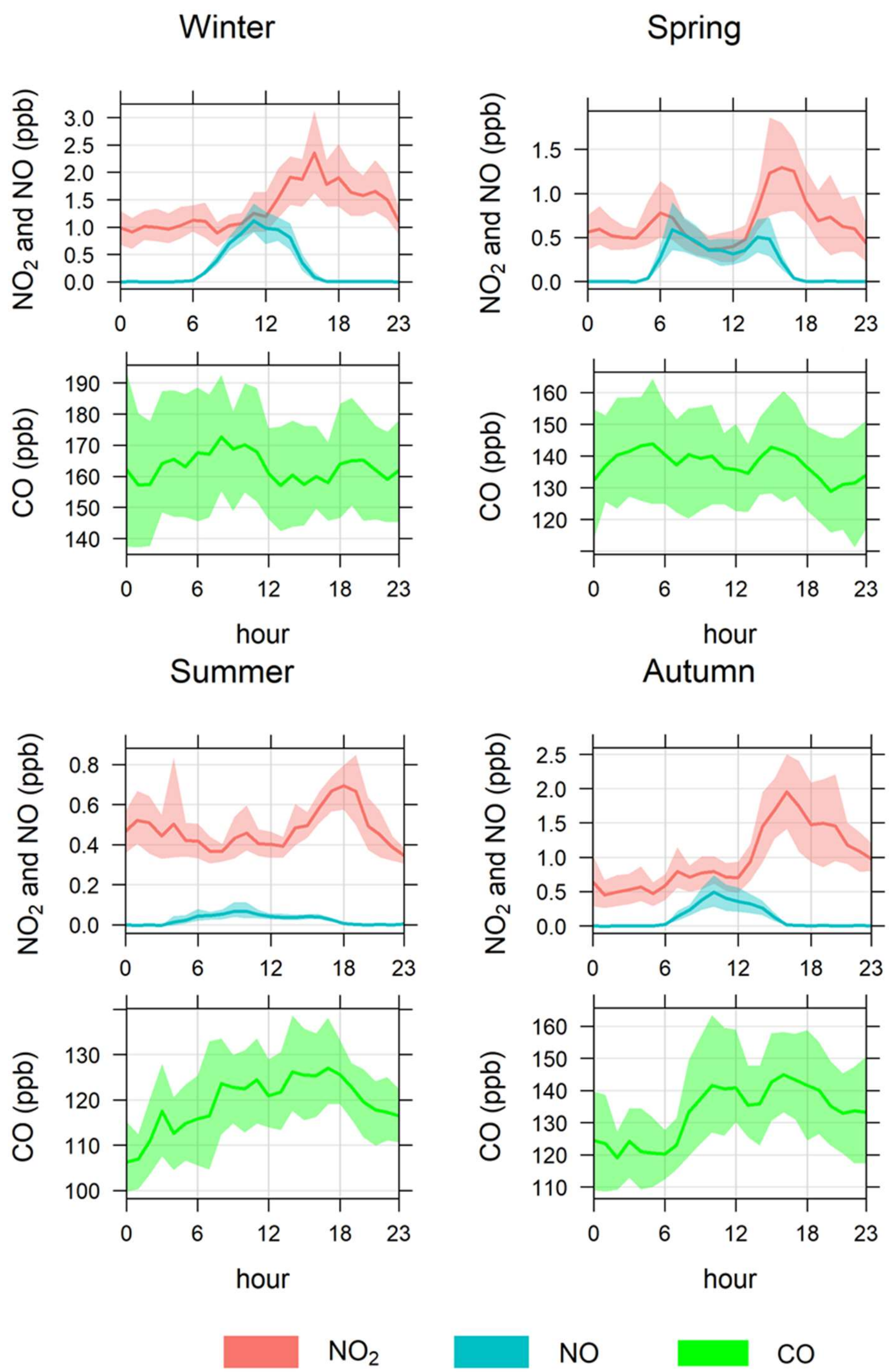

Figure 10. Seasonal daily cycles of NO, NO_2 and CO during the anomalous events at CMN. The shaded areas report the 95% confidence interval.

The analysis of case studies can provide a further description of the processes leading to the occurrence of "anomalous" NO_2 events at CMN. To this aim, in the following we briefly discusses the event detected on 7th September 2016 (Figure 11). According with results provided in Figure 10 and Figure 6, over the period 1st – 12th September 2016, the NO_2 variability was characterized by the systematic occurrence of a diurnal peak during the afternoon-evening, related to the advection of PBL air masses under thermal wind circulation. This is supported by similar variability in NO and SH (Fig. 11a), showing simultaneous peaks during afternoon-evening related to the transport of fresh pollution from the PBL. The daytime-nighttime

CO variability is less evident but still detectable, with higher values usually observed during the afternoon-evening at the measurement site (Fig. 11a). The highest NO_2 hourly values were clearly related to this diurnal variability. From 5th September 2016 to 8th September 2016, we observed an increase in the NO_2 baseline that was added to the typical diurnal variability. This is related with an increase of wind speed and the occurrence of wind from N-NE at the measurement site, testifying a change in the atmospheric circulation. A peak of NO and NO_2 was visible in the morning of 7th September 2016, in concomitance with relatively low SH values, which would support the presence of air masses more representative of the free troposphere at the measurement site. On 7th September 2016 (00:00 UTC, see Fig. 11b) the FLEXTRA back-trajectories indicated that air masses travelled over central and eastern Europe, a well-known source of NO_2 (Geddes et al., 2016), before crossing the Po basin and reaching CMN (note the consistency between local WD at CMN and back-trajectories points near the measurement site). On the same day (06:00 UTC, see Fig. 11c), in concomitance with the NO-NO_2 peak in the morning, the FLEXTRA back-trajectories reported air masses travelling at low altitude over Greece, the Aegean Sea and the Balkan peninsula before overpassing the Po basin and reaching CMN. In the following hours, in concomitance with the hourly peak in NO_2 (1.5 ppb) and CO (140 ppb), back-trajectories diagnosed air mass transport from Eastern Europe (Fig. 11c). As deduced by the observations performed by the MODIS sensor on board of NASA satellites "Terra" and "Aqua", during 5th – 8th September 2016, widespread open fires occurred over the Eastern Europe (especially over the western and northern coastline of the Black Sea, see Fig. 11d). This represented the second most important fire event over the region over August-September (Fig. SM11), as deduced by the analysis of the Global Fire Emissions Database (Giglio et al., 2013). A possible impact of open fires emission to CMN observations was consistently diagnosed by the NAAPS (Navy Aerosol Analysis and Prediction System) model (Ge et al., 2016): see https://www.nrlmry.navy.mil/aerosol_temp/loop_html/aer_globaer_europe_loop_2016090718.html). To summarize, it is likely that two different processes contributed to the appearance of the high NO_2 event detected at CMN on 7th September 2016: (i) transport of PBL air masses under thermal wind circulation and PBL diurnal mixing and (ii) underlying long-range transport of emission sources in the European domain which favored the increase of the NO_2 "baseline" values at CMN.

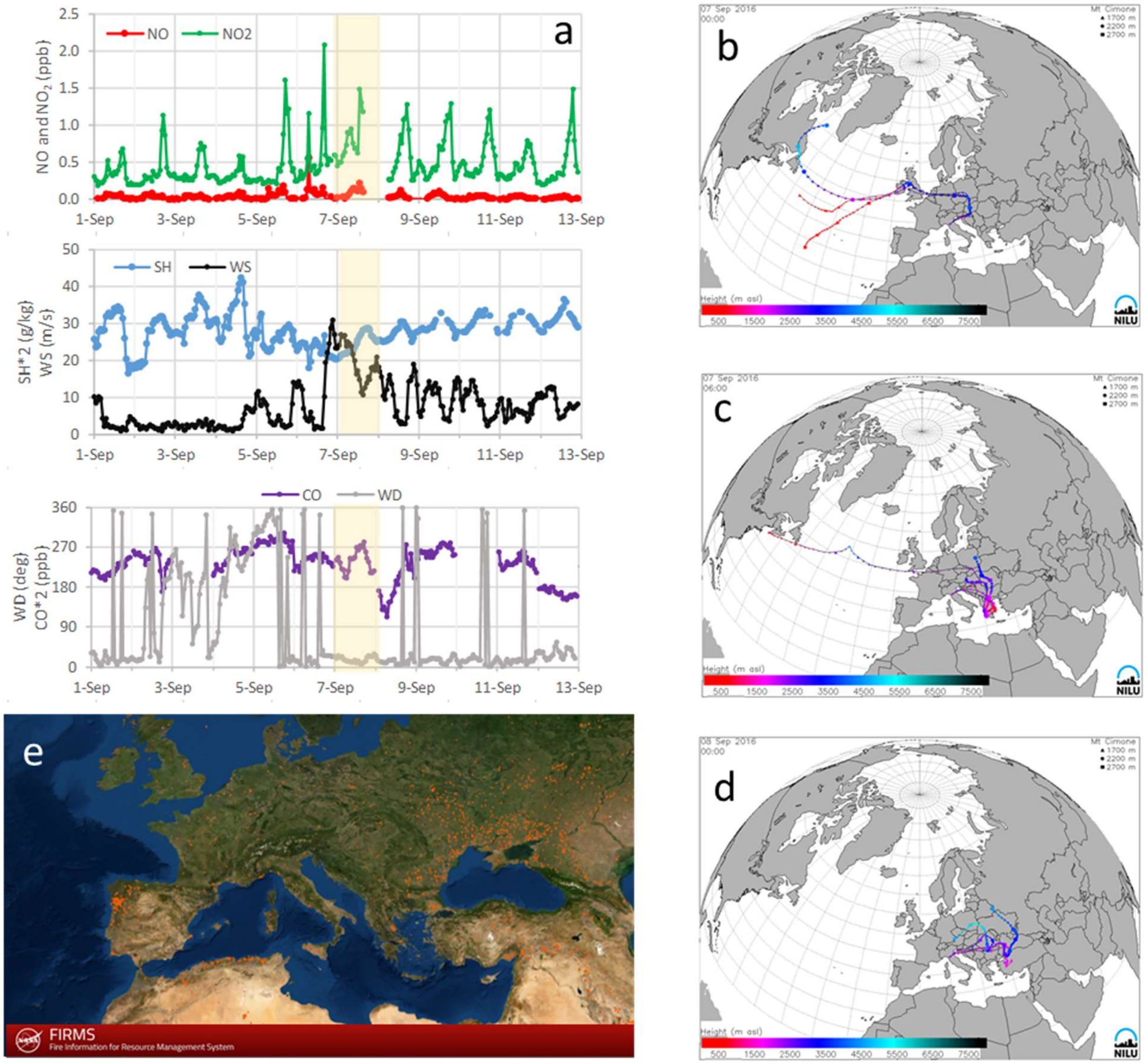

Figure 11. Observations from 1th to 12th September 2016 at CMN (plate a; the yellow area denotes the period identified as an "anomalous" NO_2 day: 7th September 2016). Plates b-d: FLEXTRA back-trajectories calculated on 7th September 2016 (00:00 UTC, plate b); on 7th September 2016 (06:00 UTC, plate c); on 8th September 2016 (00:00 UTC, plate d). MODIS fire detection by "Terra" and "Aqua" satellites cumulated over the period 5th – 8th September 2016 (from https://firms.modaps.eosdis.nasa.gov/, last accessed: 18th September 2020).

With the aim of providing hints towards the possible role of long-range atmospheric transport (i.e. on a continental scale) in driving the occurrence of anomalous NO_2 events at CMN, the $CP_{i,j}$ was calculated for the selected events on a seasonal basis (Fig. 12). While not clear patterns are evident for spring and summer, a cluster of regions with $CP_{i,j}$ exceeding 0.4 is evident for autumn and winter over eastern Europe. As deduced by the analysis of the Global Fire Emissions Database (Giglio et al., 2013), this region presents a secondary peak in the occurrence of fire number in September - October (see Fig. SM12). Thus, as already shown by the case study analysis, it can be argued that transport of air masses enriched by open fires occurring in this region can contribute to the occurrence of the anomalous NO_2 events detected at CMN during autumn.

In Bulgaria, Perrone et al. (2018) pointed out the occurrence of high biomass burning emissions related to domestic heating in winter months. This nicely fits with the high $CP_{i,j}$ values observed over the region west to the Black Sea in winter. Moreover, possible contributions from emissions linked to stationary sources and maritime traffic occurring over North-western Turkey (including the Istanbul region and the Aegean Sea) cannot be neglected (Perrone et al., 2018). By excluding 2016 from the spring-summer-autumn analysis, we found rather consistent results: indeed, we only recognized less coherent (but still present) contributions related to atmospheric circulation from the Eastern Europe during autumn (not shown).

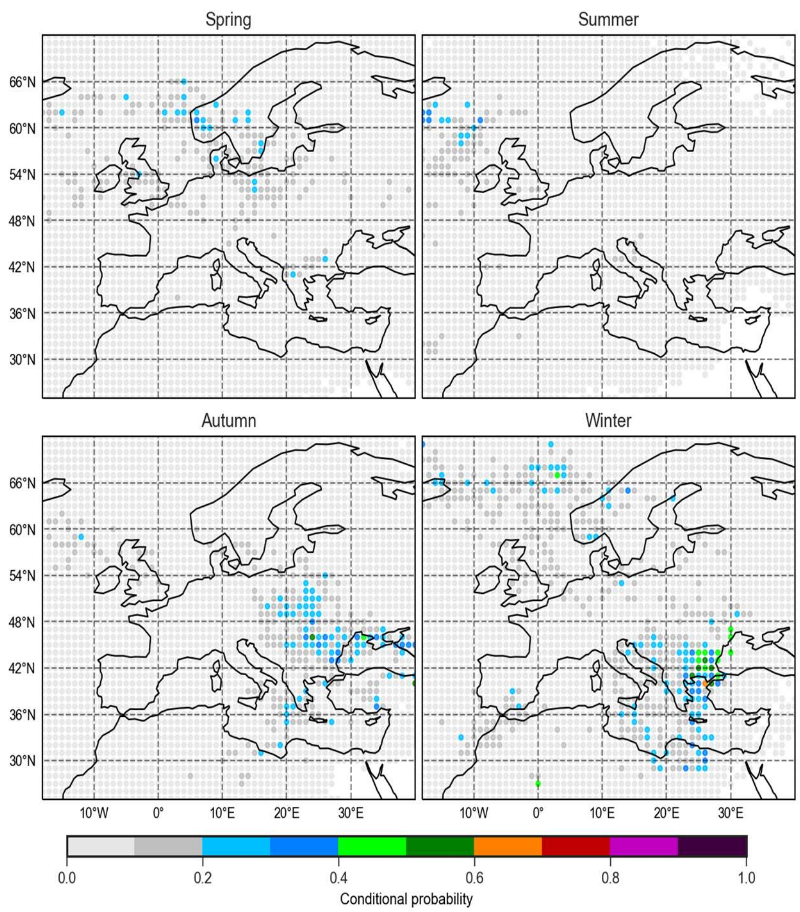

Figure 12. For the anomalous NO_2 events detected at CMN: spatial distribution of $CP_{i,j}$ reconstructed using FLEXTRA back-trajectories for each season.

3.4 Analysis of O_3/NOx ratio

Previous works (e.g. Parrish et al., 2009; Morgan et al., 2010; Rinaldi et al., 2015) used information about the variability of O_3/NO_x ratios as proxies for qualitatively evaluating the proximity to major emission sources, and to measure photochemical processing. Cristofanelli et al. (2016) used a similar approach to categorize the CMN observations during a summer field campaign, to investigate the evolution of trace gases and aerosols. Threshold values for the ratios were set to tag atmospheric observations to specific “photochemical regimes”, which would provide indirect hints about the distance from anthropogenic sources. Thus, it is interesting to systematically test the validity of this approach over the multi-annual dataset at CMN. Figure 13 reports the normalized statistical distribution of O_3/NO_x for the different seasons (NO_x was calculated as the sum of NO and NO_2 when both the species were available). For all seasons, the statistical distribution of O_3/NO_x is skewed on the right (i.e. high frequency for the low values). However, a strong seasonal variability exists for O_3/NO_x: for winter, the bulk of observations are found for ratios lower than 100, while summer shows the highest frequency of observations for values higher than 100. An intermediate situation characterized spring and autumn. This is reflected in the average values of O_3/NO_x for the different seasons, ranging from 165 in winter to 300 in summer. Due to NO_x oxidation, dilution and photochemical processes, O_3/NO_x should be higher than 10 within air masses just downwind of pollution sources, and lower than 10 for locally emitted combustion sources (Neuman et al., 2009). Based on the analysis reported in Figure 13, less than 2% of CMN observations appeared to fall in this categorization.

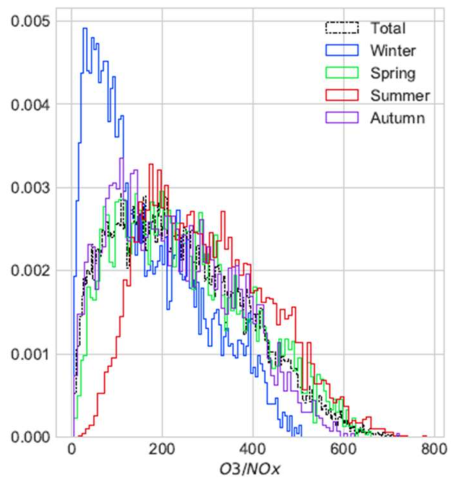

Figure 13. Normalized seasonal distributions of the hourly mean values of the ratio O_3/NO_x at CMN calculated over the period 2015 - 2019.

Following the approach by Cristofanelli et al. (2016), we analyzed the variability of CO as function of O_3/NO_x (Fig. 14), with the aim of pointing out possible discontinuities in the average CO values that should trace different fingerprints of air masses. For the relation between CO and O_3/NO_x, marked differences among the seasons were found:

- Winter and autumn showed the typical behavior reported in literature, with higher CO related to lower O_3/NO_x, thus indicating the impact of relatively "fresh" emissions. Some discontinuity points can be found, by looking at the CO average values during these seasons: $0 < O_3/NO_x < 20$, $20 < O_3/NO_x < 60$, $70 < O_3/NO_x < 100$, and $O_3/NO_x > 200$. The CO decrease with O_3/NO_x looks more linear for $20 < O_3/NO_x < 60$ in winter, and more stepwise in autumn.
- Spring presents a CO variability similar to winter-autumn, but with some specificities: it is not possible to point out a clear CO population for $0 < O_3/NO_x < 20$, and evident discontinuities exist for $O_3/NO_x = 70$ and $O_3/NO_x = 100$.
- Summer presents a rather different behavior. In general, a low number of data points fallen in the range $0 < O_3/NO_x < 70$. A linear increase affected CO values in the $40 < O_3/NO_x < 60$ range, then CO values appeared stable up to $O_3/NO_x = 400$, where a stepwise increase occurred. This is in

opposition to what shown for CMN during summer 2012 for which CO increased by the O_3/NO_x ratio (Cristofanelli et al., 2016). This behavior was robust for the single seasons from 2015 to 2018, probably related to the efficient photochemistry that affected the polluted air masses in the Mediterranean basin during summer. Indeed, the combined analysis of O_3, CO and NO_x daily mean values, clearly pointed out a concomitant and steep increase of O_3 and CO for the highest NO_x values in summer (Fig. SM13).

To shed further light on the O_3/NO_x variability observed in summer, we categorized O_3/NO_x as a function of wind direction and time of day at CMN (daytime vs nighttime, see Fig. SM14). The sector N-NE is the only one showing low O_3/NO_x values (i.e. lower than 70), pointing towards more "fresh" emissions related to the Po basin. For the N-E sectors, during daytime, this contribution represents the 10% of observations at CMN. These sectors are also characterized by a relatively large fraction of "intermediate" O_3/NO_x values (from 100 to 200), further stressing the possibility that emissions from industrialized/populated regions located upwind to CMN would affect the measurement site (Fig. SM10).

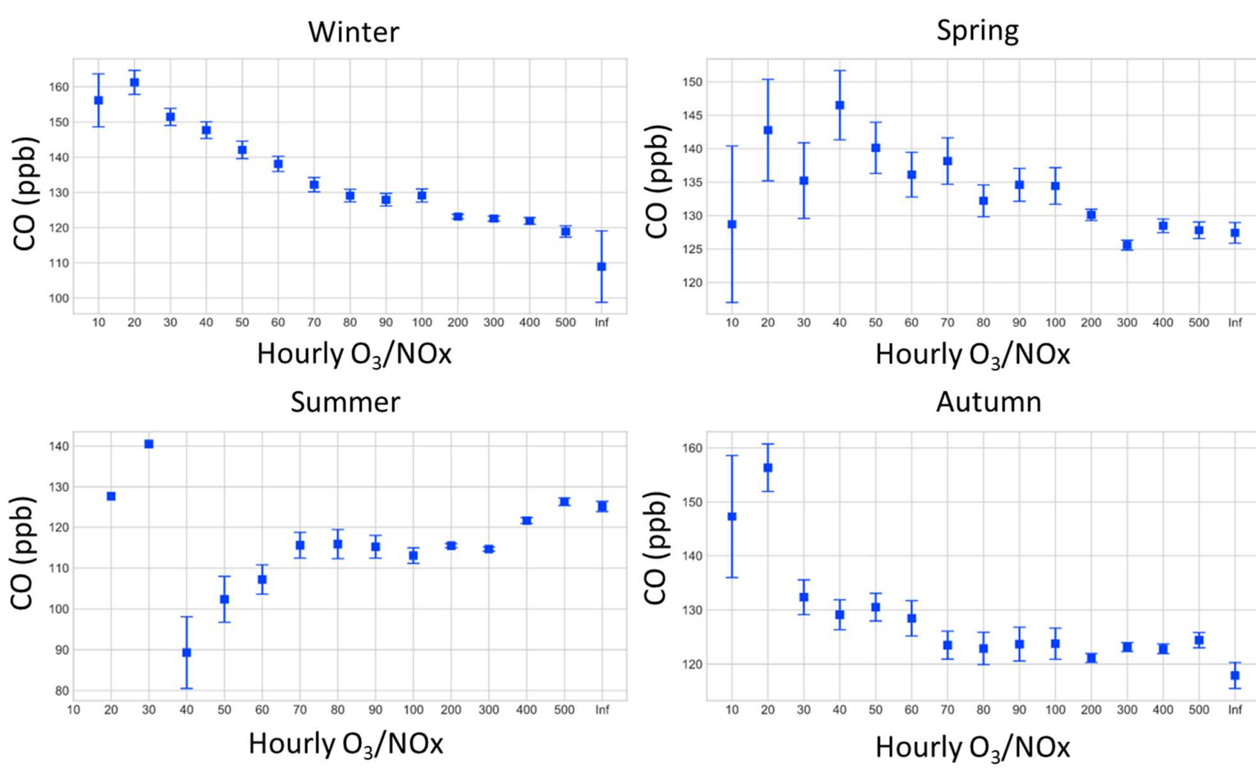

Figure 14. Relationship between CO and hourly O_3/NO_x ratio, grouped by season. Squares represent mean values for each O_3/NO_x group, and the error bars denote the uncertainty of the mean (i.e. standard deviation divided by square root of the number of values).

3.5. Free troposphere versus PBL observations

The continuous observations carried out at CMN allow to specifically investigate how NO_x varies between the "FT" and "PBL" regimes. To perform this analysis, we analyzed the hourly NO and NO_2 dataset as a function of the observation periods representative of "FT" or "PBL" conditions (Section 2.3). For comparison purposes, the same analysis was executed also for CO and the O_3/NO_x ratio (Fig. 15).

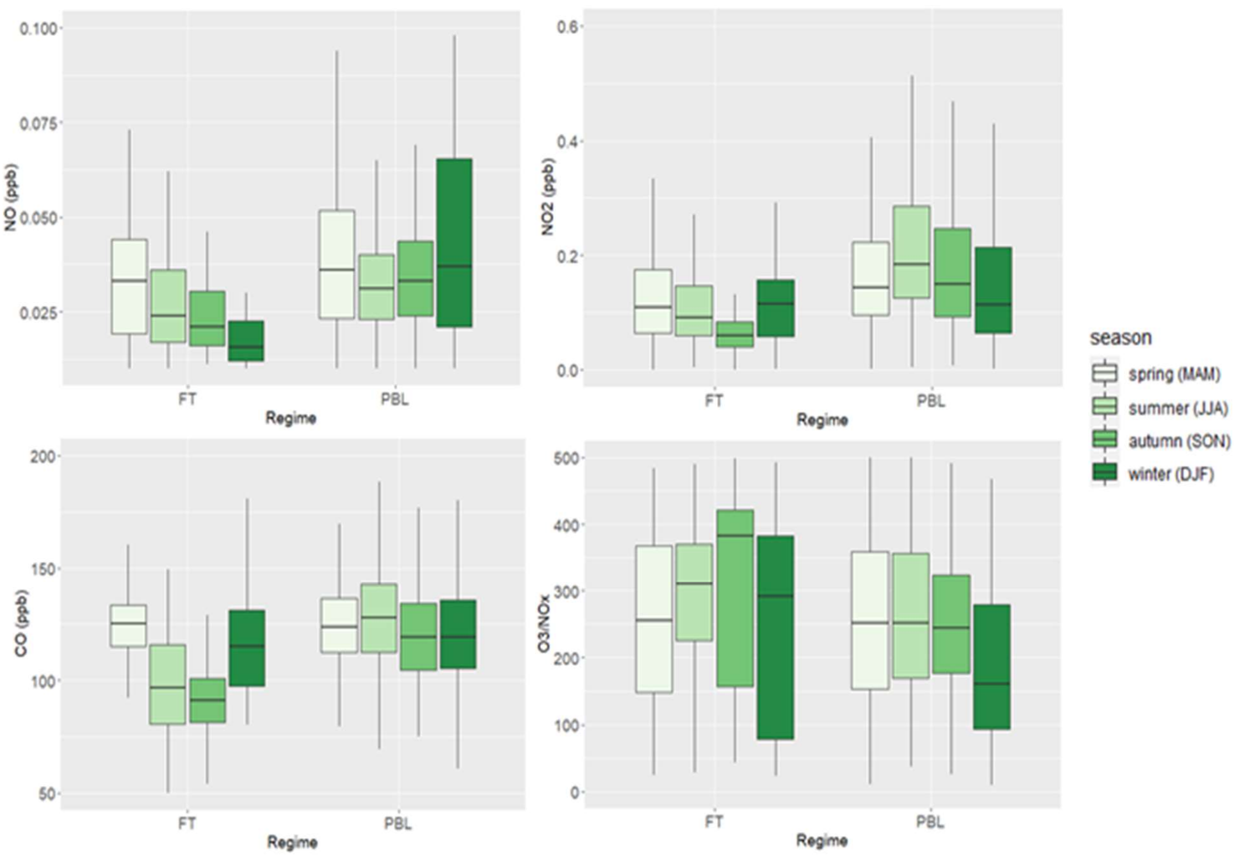

Figure 15 Comparison between the levels of NO, NO_2, CO and O_3/NO_x as a function of segregation regime ("FT", "PBL") and seasons (color scale). The box plots report the main percentiles of hourly values (5th, 25th, 75th, and 95th) and the median value (thick line).

In general, for NO, the "FT" dataset is characterized by median and percentiles values lower than the PBL dataset. This is true for all the seasons, indicating the role of regional PBL as a source of the highly reactive NO at CMN. Interestingly, the deviations between "FT" and "PBL" observations are maximized in winter when "PBL"- segregated data report median and upper percentiles more than doubled with respect to "FT" data. In the case of NO_2, the data representative for the "FT" regime were characterized by the occurrence of lower values with respect to "PBL": this is especially evident in summer and autumn. With respect to PBL-representative data, the "FT" data show lower CO values in summer and autumn, together with higher O_3/NO_x (pointing out a high degree of aging for "FT" air masses), consistent with a larger influence of polluted air masses for the "PBL"-segregated data during these seasons. For all the considered species in this analysis including O_3/NOx, the differences between "FT" and "PBL" data are minimized during spring. This further highlights the limitations related with the use of the O_3/NO_x diagnostic as (even qualitative) proxy for evaluating the closeness to emission sources.

5. Discussion and conclusions

We report an analysis of a multi-year dataset of NO_2 and NO near-surface observations at the WMO/GAW global station Mt. Cimone (CMN, Italy), covering 2015–2018. This dataset is characterized by high maturity in terms of metadata and measurement traceability. This first analysis allowed to obtain information about daily and seasonal variability of NO and NO_2 at this high mountain site (2165 m a.s.l.) overlooking the Po basin, one of the European hot-spot regions in terms of anthropogenic pollution emissions (Crippa et al., 2016).

NO and NO_2 are characterized by high values during the cold months (0.08 ppb for NO and 0.37 ppb for NO_2 in February) and low values during summer (0.02 ppb for NO and 0.18 ppb for NO_2 in July). Typical daily cycles characterized both NO and NO_2. Both seasonal and daily variability are in agreement with those observed at other remote/baseline sites in Europe, indicating that CMN observations are usually representative of the baseline atmospheric conditions (i.e. not directly impacted by anthropogenic sources). We considered the possibility that denitrification processes occurring in the mountain snowpack can affect variability of NO_x during winter and spring at CMN. Even if some events characterized by increased NO/NO_2 ratio were concomitant with snowfall events, we were not able to find out a robust relationship between snowfall and the occurrence of high NO_x events in these seasons. In 2016, with respect to the other years, higher NO_2 values were observed from May to September. Not obvious explanations related to analytical issues can be provided at this stage. Possible combined roles of transport of air masses from the regional and European PBL were suggested by the analysis of local thermal wind circulation and long-range transport by the FLEXPART dispersion model. Potential users of the CMN dataset must be cautious in using this subset of data (i.e. NO_2 for the period May - September 2016) for, e.g. model evaluation or for characterization of NO_2 mean, variability and trend.

To provide a preliminary evaluation of the impact of atmospheric transport to the seasonal NO_2 variability observed at CMN, we analyzed nighttime observations (less affected by the influence of PBL air-mass transport related to thermal wind circulation) with 3D back-trajectories. We calculated conditional probability fields ($CP_{i,j}$) for NO_2 at CMN and we performed a series of sensitivity studies to evaluate the robustness of the obtained results by varying the length of the considered back-trajectories (i.e. from 7 to 3 days) and by excluding from the analysis the CMN observations recorded from May 2016 to September 2016. Based on these analyses, we deduced that atmospheric transport from northern Africa and the Mediterranean basin represents a favorable condition for the occurrence of baseline (i.e. 0^{th} - 25^{th} percentiles) NO_2 values at CMN. The comparison of the analyses performed for the 7-day and the 3-day back-trajectories suggests that this result is more robust for spring and summer. The same comparison exercise, together with $CP_{i,j}$ calculation for CO, suggests that the occurrence of high (i.e. 75^{th} - 100^{th} percentiles) NO_2 values at CMN were robustly tagged to atmospheric circulation overpassing the central/western Europe in spring. A contribution from nearest sources (North Italy) was also evident for NO_2 in spring and summer (probably related to the more efficient vertical mixing of the lower troposphere), as deduced from $CP_{i,j,}$ calculations by using 7-day and 3-day back-trajectories. This signal over North Italy was not observed for CO. It is conceivable to suppose that the higher atmospheric lifetime of CO together with the use of nighttime back-trajectories enhanced the contributions from more distant source regions in compared with NO_2 results. High NO_2 values at CMN were related to central/western Europe also in winter and to eastern Europe in winter and summer. However, these results were obtained only for the analysis of the 7-day back-trajectories and thus can be considered less robust or, alternatively, they can trace re-emission of NO_2 from "reservoir" species (especially in spring and summer).

However, the conditional probability analysis used in this work can be affected by some caveats that underpin the "preliminary" nature of this assessment. Even if only nighttime observations were used, an interference by nighttime residual layers reminiscent of the day-time vertical convection over northern Italy cannot be completely neglected (Bonasoni et al., 2000). The conditional probability field indicates the geographic origin of the air masses but does not necessarily indicate a source location (which can effectively occur upwind or downwind of the high conditional probability region, especially when dealing with secondary pollutants or with regions crossed by a low number of back-trajectories). Moreover, it should be specified that regions characterized by high CP values but with a low frequency of back-trajectory occurrence (e.g. "peripheral" regions located at the external border of the analysis domain) likely provide only a limited integral contribution to the variability of NO_2 observed at CMN. A further point that should be considered is that, by our approach, NO_2 is considered like a "passive" tracer, and a series of processes cannot be taken into account, e.g.: oxidation, re-emission by reservoir species like PAN, impact of meteorology on actinic fluxes (and then photochemistry). Finally, the obtained results can be considered representative for the CMN but cannot be extended to other measurement locations.

The analysis of 56 days characterized by high NO_2 values suggested that transport of fresh polluted air masses from northern Italy can represent a main driving process, especially in summer and autumn. However, as deduced by perturbed diel NO_2 and CO cycles and by the analysis of 3D back-trajectories, the role of long-range transport cannot be ruled out (which can also explain the high NO_2 values observed with wind from NE in winter).

We evaluated the effectiveness of a widely used diagnostic (i.e. the O_3/NO_x ratio) in providing information and categorization of air masses as a function of the photochemical aging. Among the different seasons, we found marked differences for the relationship between CO and O_3/NO_x. This suggests that it is not possible to define a unique set of O_3/NO_x threshold values able to discriminate the photochemical aging of air masses, but that these values must be tuned as a function of the season and, possibly, of the measurement sites. As concerning the CMN case, this diagnostic was not effective in discriminating air masses tagged to "FT" or "PBL" regimes, as deduced by the combined analysis of local WS and SH.

Finally, the segregation of data as a function of conditions representative for the presence of free tropospheric or PBL-affected air masses at CMN, allowed a first characterization of air masses fingerprints as a function of these different regimes. It should be considered that our methodology (as any other possible selection methodology) cannot be considered free from erroneous cases of regime attribution. Nevertheless,

high NOx values were observed under conditions representative for transport of air masses from PBL. The differences between the two regimes are maximized in winter for NO and in summer-autumn for NO_2.
Further work is needed to provide an even more robust characterization of the presented dataset. As an instance, the investigation of NO and NO_2 variability by using the Leighton mechanism (Ridley et al. 2000; Reed et al., 2016) or by the support of an atmospheric chemistry model will be pursued in the next future.
The presented dataset is not exempt by weakness (i.e. the experimental set-up is at the limit of usability for a semi-remote location like CMN) but, in our opinion, it represents a reasonable compromise between the possibility of obtaining robust, reliable and well traced NO_x measurements with an affordable human and financial efforts. The measurements presented in this work are executed in a completely automated way, without the constant intervention of in-situ personnel and with a rather budgetary instrumentation. Probably, this dataset will never reach the absolute levels of quality of similar datasets obtained at laboratories equipped with more performing instrumentation (in terms of analytical performances) and with in-situ personnel constantly taking care of the instrumentation and materials but, nevertheless, it provides information with a reasonable level of maturity as concerning data coverage, metrological uncertainty, traceability of the data generation processes, data documentation, and data accessibility. The results achieved at CMN are promising in terms of implementing a denser network of mature continuous NO_x measurements with high temporal frequency in Italy and Europe, as promoted by the implementation of the ACTRIS Research Infrastructure (www.actris.eu). This would represent a notable contribution in the field of science services like (among others): the monitoring of the frequency of pollution episodes, the analysis of long-term trends, the provision of near-real time data for assimilation in forecast model or for model verification and the combination of NO_2 measurements from satellites sensors of new generation like TROPOMI (Veefkind et al., 2012).

Acknowledgements

CNR-ISAC strongly acknowledges the logistic cooperation of the Italian Air Force (CAMM Monte Cimone) at the Mt. Cimone station. Air mass back-trajectories are calculated using the Flextra model developed by Andreas Stohl (NILU) in cooperation with Gerhard Wotawa and Petra Seibert (Institute of Meteorology and Geophysics, Vienna) and using meteorological data provided from the ECMWF (European Centre for Medium Range Weather Forecast). FLEXTRA dataset are made available by NILU throughout https://projects.nilu.no//ccc/trajectories/. Thanks to ESA for the development of TROPOMI instrument and Copernicus for the free access to NO_2 products. The authors gratefully acknowledge "Regione Carabinieri Forestale Emilia – Romagna, Gruppo di Bologna – Centro Settore Meteomont" for providing the snow data at Pian Cavallaro. NO and NO_2 observations at CMN have been started in the framework of the National Project of Interest Nextdata, funded by MIUR (Italian Ministry for Education, University and Research), and supported by ACTRIS-2 (H2020, grant agreement No 654109) and JRU "ICOS Italy" (funded by MUR trough CNR-DTA).

References

Adame, J.A., Hernández-Ceballos, M.Á., Sorribas, M., Lozano, A. and Morena, B.A.D.l., 2014. Weekend-Weekday Effect Assessment for O_3, NOx, CO and PM10 in Andalusia, Spain (2003 - 2008). Aerosol. Air. Qual. Res., 14, 1862-1874. doi: 10.4209/aaqr.2014.02.0026.

Adame, J.A, Notario, A., Cuevas, C.A., Lozano, A., Yela, M., Saiz-Lopez, A., 2019. Recent increase in NO_2 levels in the southeast of the Iberian Peninsula. Sci. Tot. Environ., 693, 133587, doi.org/10.1016/j.scitotenv.2019.133587.

Adame, J.A., Gutierrez-Alvarez, I., Bolivar, J.P., Yela, M., 2020. Ground-based and OMI-TROPOMI NO_2 measurements at El Arenosillo observatory: Unexpected upward trends. Environ. Poll., 264, 114771, doi.org/10.1016/j.envpol.2020.114771.

Ashbaugh, L. L., Malm, W. C, Sadeh, W. Z., A residence time probability analysis of sulfur concentrations at grand Canyon National Park (1967), 1985. Atmos. Environ., 19, 8 1263-1270, https://doi.org/10.1016/0004-6981(85)90256-2.

Bonasoni, P., Stohl, A., Cristofanelli, P., Calzolari, F., Colombo, T., and Evangelisti, F., 2000. Background ozone variations at Mt. Cimone Station. Atmos. Environ., 34, 5183–5189.

Castellanos, P., and Boersma, K., 2012. Reductions in nitrogen oxides over Europe driven by environmental policy and economic recession, Sci. Rep., 2, 265. DOI: https://doi.org/10.1038/srep00265.

Colette et al., 2016. Air pollution trends in the EMEP region between 1990 and 2012 EMEP: CCC-Report 1/2016. http://nora.nerc.ac.uk/id/eprint/513779

Cooper, OR, Schultz, MG, Schroeder, S, Chang, K-L, Gaudel, A, Benítez, GC, Cuevas, E, Fröhlich, M, Galbally, IE, Molloy, S, Kubistin, D, Lu, X, McClure-Begley, A, Nédélec, P, O'Brien, J, Oltmans, SJ, Petropavlovskikh, I, Ries, L, Senik, I, Sjöberg, K, Solberg, S, Spain, GT, Spangl, W, Steinbacher, M, Tarasick, D, Thouret, V and Xu, X. et al. 2020. Multi-decadal surface ozone trends at globally distributed remote locations. Elem Sci Anth 8(1): 23. DOI: https://doi.org/10.1525/elementa.420

Crippa, M., Janssens-Maenhout, G., Dentener, F., Guizzardi, D., Sindelarova, K., Muntean, M., Van Dingenen, R., and Granier, C., 2016. Forty years of improvements in European air quality: regional policy-industry interactions with global impacts. Atmos. Chem. Phys., 16, 3825-3841, doi.org/10.5194/acp-16-3825-2016.

Cristofanelli, P., Landi, T.C., Calzolari, F., Duchi, R., Marinoni, A., Rinaldi, M., Bonasoni, P., 2016. Summer atmospheric composition over the Mediterranean basin: Investigation on transport processes and pollutant export to the free troposphere by observations at the WMO/GAW Mt. Cimone global station (Italy, 2165 m a.s.l.). Atmos. Environ., *141*, 139-152, doi.org/10.1016/j.atmosenv.2016.06.048.

Cristofanelli, P., et al., 2017. Investigation of reactive gases and methane variability in the coastal boundary layer of the central Mediterranean basin. Elem. Sci. Anth., 5, 12, doi.org/10.1525/elementa.216.

Cristofanelli, P., Brattich, E., Decesari, S., Landi, T.C., Maione, M., Putero, D., Tositti, L., Bonasoni, P., 2018. High Mountain Atmospheric Research—The Italian Mt. Cimone WMO/GAW Global Station (2165 m a.s.l.). Springer: Amsterdam, The Netherland, pp. 1–135.

Cuevas, C., Notario, A., Adame, J. et al., 2015. Evolution of NO_2 levels in Spain from 1996 to 2012. Sci Rep. 4, 5887, https://doi.org/10.1038/srep05887.

Fischer, E.V., Jacob, D.J., Yantosca, R.M., Sulprizio, M.P., Millet, D.B., et al., 2014. Atmospheric peroxyacetyl nitrate (PAN): a global budget and source attribution. Atmos. Chem. Phys., 14(5), 2679–2698. doi: 10.5194/acp-14-2679-2014.

Ge, C., J. Wang, J. S. Reid, D. J. Posselt,P. Xian, and E. Hyer, 2017. Mesoscalemodeling of smoke transport fromequatorial Southeast Asian MaritimeContinent to the Philippines: First com-parison of ensemble analysis with in situobservation., J. Geophys. Res. Atmos., 122, 5380–5398. doi:10.1002/2016JD026241.

Geddes, J.A., Martin, R.V., Boys, B.L., van Donkelaar, A., 2016. Long-Term Trends Worldwide in Ambient NO_2 Concentrations Inferred from Satellite. Observations. Environ. Health Perspect., 124, 3, https://doi.org/10.1289/ehp.1409567.

Georgoulias, A. K., van der A, R. J., Stammes, P., et al., 2019. Trends and trend reversal detection in 2 decades of tropospheric NO2 satellite observations. Atmos. Chem. Phys., 19, 6269-6294. DOI: https://doi.org/10.5194/acp-19-6269-2019.

Giglio, L., Randerson, J. T., and van der Werf, G. R., 2013. Analysis of daily, monthly, and annual burned area using the fourth-generation global fire emissions database (GFED4). J. Geophys. Res. Biogeosci., 118, 317– 328, doi:10.1002/jgrg.20042.

Gilge, S., Plass-Duelmer, C., Fricke, W., Kaiser, A., Ries, L., Buchmann, B., and Steinbacher, M., 2010. Ozone, carbon monoxide and nitrogen oxides time series at four alpine GAW mountain stations in central Europe. Atmos. Chem. Phys., 10, 12295–12316, https://doi.org/10.5194/acp-10-12295-2010.

Gilge, S., Plass-Duelmer, C., Roher, F., Steinbacher, M., Fjaeraa, A.M., Lageler, F., Walden, J. WP4- NA4: Trace gases networking: Volatile organic carbon and nitrogen oxides -Deliverable D4.10: Standardized operating procedures (SOPs) for NOxy measurements. Deliverable WP4 / D4.10 (M42).2014. Version: 2014/09/19, last accessed: May 2020. http://fp7.actris.eu/Portals/97/deliverables/PU/WP4_D4.10_M42.pdf.

Giorgi F., and Lionello P., 2008. Climate change projections for the Mediterranean region. Glob. Planet. Chang., 63, 90–104.

Henne, S., Brunner, D., Folini, D., Solberg, S., Klausen, J., and Buchmann, B., 2010: Assessment of parameters describing representativeness of air quality in-situ measurement sites. Atmos. Chem. Phys., 10, 3561–3581, https://doi.org/10.5194/acp-10-3561-2010.

Honrath, R. E., Peterson, M. C., Dziobak, M. P., Dibb, J. E., Arsenault, M. A., and Green, S. A.: Release of NOx from sunlightirradiated midlatitude snow, Geophys. Res. Lett., 27(15), 2237– 2240, 2000.

McClure, C.D., Jaffe, D.A. and Gao, H. (2016). Carbon Dioxide in the Free Troposphere and Boundary Layer at the Mt. Bachelor Observatory. Aerosol Air Qual. Res. 16: 717-728. https://doi.org/10.4209/aaqr.2015.05.0323

Monks, P.S., Granier, C., Fuzzi., S., Stohl, A., Williams, M.L., et al., 2009. Atmospheric composition change – global and regional air quality. Atmos Environ 43, 5268-5350.

Morgan, W. T., Allan, J. D., Bower, K. N., Highwood, E. J., Liu, D., McMeeking, G. R., Northway, M. J., Williams, P. I., Krejci, R., and Coe, H., 2010. Airborne measurements of the spatial distribution of aerosol chemical composition across Europe and evolution of the organic fraction. Atmos. Chem. Phys., 10, 4065–4083, https://doi.org/10.5194/acp-10-4065-2010.

Naitza, L., Cristofanelli, P., Marinoni, A., Calzolari, F., Roccato, F., Busetto, M., Sferlazzo, D., Aruffo, E., Di Carlo, P., Bencardino, M., D'Amore, F., Sprovieri, F., Pirrone, N., Dallo, F., Gabrieli, J., Vardè, M., Resci, G., Barbante, C., Bonasoni, P., Putero, D., 2020. Increasing the maturity of measurements of essential climate variables (ECVs) at Italian atmospheric WMO/GAW observatories by implementing automated data elaboration chains. Computers & Geosciences, 137, 104432, doi: 10.1016/j.cageo.2020.104432.

Neuman, J. A., Nowak J. B., Zheng W., Flocke F., Ryerson T. B., Trainer M., Holloway J. S., Parrish D. D., Frost G. J., Peischl J., Atlas E. L., Bahreini R., Wollny A. G., and Fehsenfeld F. C., 2009. Relationship between photochemical ozone production and NOx oxidation in Houston, Texas. J. Geophys. Res., 114, D00F08, doi:10.1029/2008JD011688.

Okamoto, S., Tanimoto, H. A review of atmospheric chemistry observations at mountain sites. Prog. in Earth and Planet. Sci. 3, 34 (2016). https://doi.org/10.1186/s40645-016-0109-2

Pandey Deolal, S., Brunner, D., Steinbacher, M., Weers, U., and Staehelin, J.: Long-term in situ measurements of NOx and NOy at Jungfraujoch 1998–2009, 2012. time series analysis and evaluation. Atmos. Chem. Phys., 12, 2551–2566, https://doi.org/10.5194/acp-12-2551-2012.

Parrish, D., Allen, D., Bates, T., Fehsenfeld, F., Feingold, G., Ferrare, R., Hardesty, R., Meagher, J., Nielsen-Gammon, J., Pierce, R., Ryerson, T., Seinfeld, J., Williams, E., 2009. Overview of the Second Texas Air Quality Study (TexAQS II) and the Gulf of Mexico Atmospheric Composition and Climate Study (GoMACCS). J. Geophys. Res., 114, D00F13, doi:10.1029/2009JD011842.

Perrone, M.G., Vratolis, S., Georgieva, E., Török, S., Šega, K., Veleva, B., Osán, J., Bešlić, I., Kertész, Z., Pernigotti, D., Eleftheriadis, K., Belis, C.A., 2018. Sources and geographic origin of particulate matter in urban areas of the Danube macro-region: The cases of Zagreb (Croatia), Budapest (Hungary) and Sofia (Bulgaria), Sci. Tot. Environ., 619–620, doi.org/10.1016/j.scitotenv.2017.11.092.

Reed, C., Evans, M. J., Di Carlo, P., Lee, J. D., and Carpenter, L. J.: Interferences in photolytic NO2 measurements: explanation for an apparent missing oxidant?, Atmos. Chem. Phys., 16, 4707–4724, https://doi.org/10.5194/acp-16-4707-2016, 2016.

Reidmiller, D. R., Jaffe, D. A., Fischer, E. V., and Finley, B.: Nitrogen oxides in the boundary layer and free troposphere at the Mt. Bachelor Observatory, Atmos. Chem. Phys., 10, 6043–6062, https://doi.org/10.5194/acp-10-6043-2010, 2010.

Reuter, M., Buchwitz, M., Schneising, O., Krautwurst, S., O'Dell, C. W., Richter, A., Bovensmann, H., and Burrows, J. P., 2019. Towards monitoring localized CO_2 emissions from space: co-located regional CO_2 and NO_2 enhancements observed by the OCO-2 and S5P satellites, Atmos. Chem. Phys., 19, 9371–9383, https://doi.org/10.5194/acp-19-9371-2019.

Rinaldi, M., Gilardoni, S., Paglione, M., Sandrini, S., Sandro, F., Massoli, P., Bonasoni, P., Cristofanelli, P., Marinoni, A., Poluzzi, V., Decesari, S., 2015. Organic aerosol evolution and transport observed at Mt. Cimone (2165 m a.s.l.), Italy, during the PEGASOS campaign. Atmos. Chem. Phys., 15. 10.5194/acp-15-11327-2015.

Ridley, B., Walega, J., Montzka, D., Grahek, F., Atlas, E., Flocke, F., Stroud, V., Deary, J., Gallant, A., Boudries, H., Bottenheim, J., Anlauf, K., Worthy, D., Sumner, A., Splawn, B., and Shepson, P.: Is the Arctic surface layer a source and sink of NOx in winter/spring, J. Atmos. Chem., 36, 1–22, 2000.

Schultz, M.G., Akimoto, H., Bottenheim, J., Buchmann, B., Galbally, I.E., Gilge, S., Helmig, D., Koide, H., Lewis, A.C., Novelli, P.C., Plass- Dülmer, C., Ryerson, T.B., Steinbacher, M., Steinbrecher, R., Tarasova, O., Tørseth, K., Thouret, V. and Zellweger, C., 2015. The Global Atmosphere Watch reactive gases measurement network. Elem Sci Anth, 3, 67, doi.org/10.12952/journal.elementa.000067.

Stohl, A., Wotawa, G., Seibert, P., and Kromp-Kolb, H., 1995. Interpolation errors in wind fields as a function of spatial and temporal resolution and their impact on different types of kinematic trajectories. J. Appl. Meteor., 34, 2149-2165.

Stohl, A., and Seibert, P., 1998. Accuracy of trajectories as determined from the conservation of meteorological tracers. Q. J. Roy. Met. Soc., 124, 1465-1484.

Stohl, A, Hittenberger, M, Wotawa, G. 1998. Validation of the Lagrangian particle dispersion model FLEXPART against large scale tracer experiments. Atmos Environ 24: 4245-4264. DOI: 10.1016/S1352-2310(98)00184-8

Stohl, A, Forster, C, Frank, A, Seibert, P, Wotawa, G, 2005. Technical note: The Lagrangian particle dispersion model FLEXPART version 6.2. Atmos Chem Phys 5: 2461–2474.

Veefkind, J.P., Aben, I., McMullan, K., F€orster, H., De Vries, J., Otter, G., Claas, J., Eskes, H.J., de Haan, J.F., Kleipool, Q., van Weele, M., Hasekamp, O., Hoogeveen, R., Landgraf, J., Snel, R., Tol, P., Ingmann, P., Voors, R., Kruizinga, B., Vink, R., Visser, H., Levelt, P.F., Veefkind, J.P., Aben, I., McMullan, K., et al., 2012. TROPOMI on the ESA Sentinel-5 Precursor: a GMES mission for global observations of the atmospheric composition for climate, air quality and ozone layer applications. Remote Sens. Environ. 120 (2012), 70. https://doi.org/10.1016/ j.rse.2011.09.027.

Waked et al., 2018. Investigation of the geographical origins of PM10 based on long, medium and short-range air mass back-trajectories impacting Northern France, during the period 2009-2013. Atmos. Env., 193, 143-152. DOI: https://doi.org/10.1016/j.atmosenv.2018.08.015

Zanis, P., Monks, P.S., Schuepbach, E. et al. The Role of In Situ Photochemistry in the Control of Ozone during Spring at the Jungfraujoch (3,580 m asl) – Comparison of Model Results with Measurements. Journal of Atmospheric Chemistry 37, 1–27 (2000). https://doi.org/10.1023/A:1006349926926

Zellweger, C., Steinbacher, M., Buchmann, B., Steinbrecher, R., 2018. System and performance audit for surface ozone, carbon monoxide, methane, carbon dioxide and nitrous oxide at the global GAW station Mt. Cimone Italy June, 2018. Dübendorf Switzerland: EMPA: WCC-Empa Report 18/1. Available at https://www.empa.ch/web/s503/wcc-empa.